Invariants and Constructions of Knotted Surfaces in 4-manifolds

by

Devashi Gulati

(Under the Direction of Peter Lambert-Cole)

Abstract

This dissertation explores bridge n-sections of knotted surfaces in 4-manifolds by defining invariants that measure the complexity of their topology and by giving geometric constructions that determine Lagrangian surfaces in 4-manifolds under certain conditions.

First, we present an elegant geometric construction that generates all triple grid diagrams. A triple grid diagram is a combinatorial representation of certain knotted surfaces in $\mathbb{CP}^2$, which can determine a Lagrangian surface under specific conditions. Previously, only a few examples of triple grid diagrams were known, and no efficient method for producing examples existed. Our key insight is to approach the search by focusing on the abstract, Tait-colored cubic graph Γ that we aim to realize through a triple grid diagram, rather than conditioning on the grid size n. From this viewpoint, the problem reduces to pure linear algebra and can be solved efficiently in polynomial time, as compared to testing pairs of permutations, which requires $O((n!)^2)$-time. This work is a collaboration with Lambert-Cole.

Second, we define invariants $\mathcal{L}^*$ and $\mathcal{L}^{\mathcal{P}}$ of bridge n-sections of knotted surfaces in 4-manifolds. These invariants measure the complexity of knotted surfaces in terms of paths in the dual cut complex and pants complex, respectively, of a closed, oriented surface. These invariants generalize previous $\mathcal{L}$-invariants for trisected 4-manifolds. We establish fundamental properties of these invariants, distinguish them from previous $\mathcal{L}$-invariants, and compute them for several explicit examples. Additionally, we prove that these invariants detect unknotted surfaces in certain 4-manifolds. This is joint work with Aranda, Blackwell, Karimi, Kim, Meyer and Pongtanapaisan.

Third, we introduce quadruple grid diagrams for the 4-section of $\mathbb{CP}^1 \times \mathbb{CP}^1$, analogous to triple grid diagrams for $\mathbb{CP}^2$. Due to their highly symmetric nature, we modify the construction to define quasiquadruple grid diagrams. The additional flexibility of quasiquadruple grid

diagrams has the ability to determine embedded Lagrangian surfaces in $\mathbb{CP}^1 \times \mathbb{CP}^1$ under certain conditions, following an adapted version of the similar construction for triple grid diagrams. Furthermore, we generalize the notion to define geometric n-tuple grid diagrams for toric sympletic manifolds. This work is joint with Fushida-Hardy and Wakelin.

INDEX WORDS: [Low-dimensional topology, Smooth 4-manifolds, Trisections, Bridge n-sections, Knotted surfaces, Lagrangian surfaces, Contact Topology, Grid diagrams, Graph Theory]

Invariants and Constructions of Knotted Surfaces in 4-manifolds

by

Devashi Gulati

M.Sc. Hons. Mathematics, BITS Pilani, India, 2019
B.E. Hons. Computer Science, BITS Pilani, India, 2019

A Dissertation Submitted to the Graduate Faculty of the
University of Georgia in Partial Fulfillment of the Requirements for the
Degree.

DOCTOR OF PHILOSOPHY

Athens, Georgia

2024

Invariants and Constructions of Knotted Surfaces in 4-manifolds

by

Devashi Gulati

Major Professor: Peter Lambert-Cole

Committee: Akram Alishahi
David Gay
Gordana Matic

Electronic Version Approved:

Ron Walcott
Dean of the Graduate School
The University of Georgia
August 2024

Dedication

I dedicate this work to my parents, who have given me unwavering support and love throughout my life. Also, I dedicate this work to my extended family, who have always been encouraging and supportive of my academic endeavours.

Acknowledgments

I am very fortunate to have had a lot of support during my Ph.D. journey. First and foremost, I would like to thank my advisor, Peter Lambert-Cole, for his constant encouragement and guidance. There have been countless times during my Ph.D. when I have felt grateful to have him as my advisor due to his kindness, patience, and tremendous support. Discussing mathematics with him has been both fun and motivating.

Next, I would like to extend my gratitude to my committee members: David Gay, Akram Alishahi, and Gordana Matic. David Gay, thank you for motivating me towards algebraic topology with your enthusiasm and for fostering a supportive community of graduate students in topology at UGA. Akram Alishahi, thank you for teaching me many things through many courses over the years. Lastly, I am grateful to Gordana Matic for her interest in my research and our stimulating mathematical conversations. I would like to thank you all for always having your door open to answer math questions.

I would also like to thank Mike Usher, Neil Lyall, Pete Clark, Daniel Nakano, Shuzhou Wang, and Alexander Petukhov for teaching me foundational courses, as well as all the math faculty at UGA for their support. Additionally, I am grateful to the administrative staff for their patience and encouragement: Laura Ackerley, Christy McDonald, Lucy Barrera, and Rinakia Jones.

Thank you to the topology graduate students at UGA for all the math conversations, guidance, and encouragement: Sarah Blackwell, Swapnanil Banerjee, Terrin Warren, Geunyoung Kim, and Daniel Hartman.

This dissertation would not have been possible without my collaborators: Román Aranda, Sarah Blackwell, Shintaro Fushida-Hardy, Homayun Karimi, Geunyoung Kim, Nicholas Paul Meyer, Puttipong Pongtanapaisan, and Laura Wakelin. I really enjoyed talking and doing mathematics with you all.

I would like to thank all of my fellow graduate students, especially Alex (Brower), Alex (Tepper), Cameron, Dustin, Ernest, Gabe, Gary, Han, Ilkiz, Komal, Lauren, Micheala, Peter (Woolfitt), Raemeon, Reddy, Rishika, Sayan, Sarah, Swaroop, Swapnanil, Terrin, and Ye Tian.

Special mention to Hannah. Expressing all my gratitude will take pages, so I will just tell y'all individually.

I have been fortunate to have had many supportive people apart from the math world, thanking whom will be a chapter in itself. I will mention here the community of Indian graduate students I have met through UGA, especially: Subham, Sayani, Anushka, Anant, Jeevan, Sneha, Swapnanil, Aditi, and Rajani. Thank you for the support and dinners.

I would like to end by thanking my parents and extended family for their support, and my best friend Swati Hans, who is basically family. I would also like to thank (Shreya) Arya and Dipali Swain, fellow math Ph.D.s, for our weekly conversations. I have been fortunate to have had them by my side since I started my math journey at BITS Pilani.

Contents

List of Figures

List of Tables

Chapter 1

Introduction

Spaces of dimension less than four can be can be envisioned completely. Studying four dimensional manifolds requires some method of capturing their properties via lower-dimensional manifolds. One way to understand the properties of 4-manifolds is via the properties of knotted surfaces in 4-manifolds.

As it is difficult to visualize 4-manifolds, we study them via projections and decompositions. In 2016, Gay and Kirby introduces trisections of 4-manifolds [GK16], a higher dimensional analogue of Heegaard decompositions of 3-manifolds. This decomposition of every smooth, closed, connected, oriented 4-manifolds into three elementary pieces captures the topological complexity of the manifold via curves on a 2-dimensional surface. This was extended to bridge trisections of 4-manifolds in 2018 by Meier and Zupan [MZ18] to capture the topological complexity of knotted surfaces in 4-manifolds via arcs and curves on 2-dimensional surfaces.

On a different note, a grid is a computer-friendly way to encode knots and links in S^3. A grid diagram is a collection of points on a grid such that each row and column of the grid contains exactly two points. Moreover, rotating a grid diagram by 45° produces a front projection of a Legendrian link in the standard tight contact structure on S^3. Every smooth link and every Legendrian link can be described by some grid diagram.

Blackwell, Gay and Lambert-Cole defined triple grid diagrams, which encode surfaces in bridge position in $\mathbb{CP}^2$, a 4-manifold [BGL23], [Bla22]. In certain cases, a triple grid diagram determines a closed Lagrangian surface in $\mathbb{CP}^2$. Specifically, each triple grid diagram determines three grid diagrams (row-column, column-diagonal and diagonal-row) and thus three Legendrian links in the three standard contact 3-spheres of the trisection of $\mathbb{CP}^2$.

1.1 Moduli Spaces of Lagrangian Surfaces in $\mathbb{CP}^2$ obtained from Triple Grid Diagrams

From the introduction of bridge position for surfaces [MZ17a], it was immediately clear that one could define and search for 'triple grid diagrams' for surfaces in $\mathbb{CP}^2$ (with respect to the genus 1 trisection), just as there exist grid diagrams for knots and links in S^3 and lens spaces (with respect to the genus 1 Heegaard splitting). However, it proved difficult to construct examples, either by an approximation method or by a combinatorial search. A grid diagram on an $n \times n$-grid can be encoded by a pair of permutations in the symmetric group S_n. But pairs that satisfy a third slope condition are sparse.

We give an elegant geometric construction that produces all triple grid diagrams. The insight is to conduct the search by conditioning on the abstract, Tait-colored cubic graph Γ one is trying to realize by a triple grid diagram, as oppposed to conditioning on the grid size n. From this perspective, the problem is purely linear algebra and can be solved quickly in polynomial time; whereas testing pairs of permutations requires $O((n!)^2)$-time. In fact, we can prove the existence of triple grid diagrams purely by counting dimensions of intersecting linear subspaces. This is joint work with Lambert-Cole [GL24].

Theorem 1.1.1. *Let Γ be an abstract Tait-colored cubic graph with $2b$ vertices. The moduli space $\mathcal{M}(\Gamma)$ of geometric triple grid diagrams with graph-type Γ is a smooth manifold.*

1. *If $b = 1$, then the moduli space is empty.*
2. *If $b = 2$, then the moduli space is 2-dimensional and consists of $\mathbb{T}^2$-translates of a single element, the $\mathbb{RP}^2$-graph in Figure 3.4.*
3. *If $b \geq 3$, then $\mathcal{M}(\Gamma)$ is nonempty and has dimension $d \geq b$.*

1.2 Pants distances of knotted surfaces in 4-manifolds

In 2018, Kirby and Thompson used trisecions to introduce an invariant of closed 4-manifolds, denoted by $\mathcal{L}(X)$, which uses the cut complex of a surface to define the distance between the three handlebodies of a trisection [KT18].

The *cut complex* $\mathscr{C}$ of Σ_g is a 1-complex with vertices corresponding to (isotopy classes) of cut systems. Two vertices α and α' in $\mathscr{C}$ are connected by an edge of type 0 if their corresponding cut systems $\alpha = \{\alpha_1, \alpha_2, \ldots, \alpha_g\}$ and $\alpha' = \{\alpha'_1, \alpha'_2, \ldots, \alpha'_g\}$ agree on $g - 1$

curves and their final curves are disjoint. Two vertices α and α' are connected by an edge of type 1 if their corresponding cut systems α and α' agree on $g-1$ curves and their final curves intersect in a single point. The distance between two vertices α and α', $d(\alpha, \alpha')$, is the length of the shortest path (using the edge-metric) connecting them in the cut complex.

In recent years, versions of the $\mathcal{L}$-invariant for other 4-dimensional structures using different complexes have been defined. For compact 4-manifolds with boundary, Castro, Islambouli, Miller and Tomova used the arc-cut complex of the relative trisections to define $\mathcal{L}$-invariants [Cas+22]. Similarly, for knotted surfaces in S^4, Blair, Campisi, Taylor, and Tomova used the pants complex and bridge trisections to formulate their version of $\mathcal{L}$-invariant [Bla+20]. Aranda, Pongtanapaisan, and Zhang used the dual curve complex and bridge trisections to define a new $\mathcal{L}^*$-invariant for knotted surfaces in S^4 [APZ22].

$\mathcal{L}$-invariants detect how complex the topology of the manifold is. For example, it has been proved that the $\mathcal{L}$-invariant of a surface in S^4 can be used to detect when a knotted surface is not prime or smoothly unknotted [Bla+20]. These findings demonstrate the potential insights of $\mathcal{L}$-invariants in the smooth topology in four dimensions.

We extended the $\mathcal{L}$-invariants of [Bla+20] and [APZ22] for knotted surfaces in arbitary 4-manifolds. The new invariants, denoted by $\mathcal{L}_n^*$ and $\mathcal{L}_n^{\mathcal{P}}$, are in the style of the bridge and pants complexities of knots in 3-manifolds studied by Johnson and Zupan in [Joh06] and [Zup13]. They are invariants of bridge n-sections of (4-manifold, surface) pairs. When the surface is not present, the invariants measure the complexity of a closed 4-manifold independent from the one originally defined by Kirby and Thompson. When the 4-manifold is S^4, the invariants $\mathcal{L}_3^{\mathcal{P}}$ and $\mathcal{L}_3^*$ agree with the invariants $\mathcal{L}$ and $\mathcal{L}^*$ of a knotted surface from [Bla+20] and [APZ22], respectively. This is joint work with Aranda, Blackwell, Karimi, Kim, Meyer and Pongtanapaisan.

1.3 Quasiquadruple grid diagrams for surfaces in $\mathbb{CP}^1 \times \mathbb{CP}^1$

A grid diagram is a collection of points on a toroidal grid which realises a link in $\mathbb{S}^3$. There is a natural way to interpret this as a front projection of a Legendian link in the standard contact $\mathbb{S}^3$. Blackwell, Gay and Lmabert-Cole defined triple grid diagrams [GK16], which give an analogous description of a surface in bridge position in $\mathbb{CP}^2$. We extend this notion to $\mathbb{CP}^1 \times \mathbb{CP}^1$, and define quadruple grid diagrams. Due to the highly symmetric nature of the 4-section, this turns out to be highly restrictive. We use a sympletic version of a polyhedral

decomposition (introduced in [Lam21]) to define quasiquadruple grid diagrams, which are more flexible. This is joint work with Fushida-Hardy and Wakelin.

Chapter 2

Background

2.1 Heegaard splittings and Heegaard Diagrams

For smooth closed 3-manifolds, Heegaard splitting is a decompsition into two elementary pieces. A *Heegaard splitting* of a compact closed oriented 3-manifold Y is a decomposition into two handlebodies, H_0 and H_1, glued along their common boundary Σ_g.

$$Y = H_0 \cup_{\Sigma_g} H_1$$

A *genus g handlebody* is diffeomorphic to the connect sum of g solid torii, having an oriented surface with genus g, Σ_g, as boundary. A *cut system* for Σ_g is a g-tuple of homologically linearly independent, pairwise disjoint, embedded curves $\gamma = \{\gamma_1, \ldots, \gamma_g\}$. A *Heegaard diagram* is a triple (Σ, α, β), where α and β are both cut systems for Σ. It encodes all the information about the Heegaard splitting of the 3-manifold.

2.1.1 Examples

The genus 1 Heegaard decomposition of S^3 corresponds to a diagram $(\Sigma_1, \alpha, \beta)$ where α and β meet transversely at a unique point. For $S^1 \times S^2$, the Heegard diagram is $(\Sigma_1, \alpha, \alpha)$. The *lens space* $L(p, q)$ has a diagram $(\Sigma_1, \alpha, \beta)$. Here, $[\alpha] = y$ and $[\beta] = px + qy$, considering a standard basis $x, y \in H_1(\Sigma_1) = \mathbb{Z} \oplus \mathbb{Z}$. α and β intersect at p points.

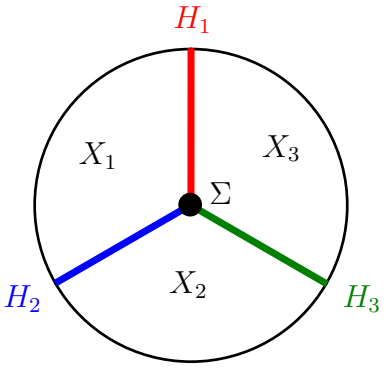

Figure 2.1: Schematic depicting the decomposition of a 4-manifold into a trisection

2.2 Trisections and Multisections

2.2.1 Trisections

Gay and Kirby introduced the notion of a trisection of a smooth closed 4-manifold, which is a 4-dimensional analogue of Heegaard splittings [GK16]. A trisection is a decomposition of the 4-manifold into three elementary pieces. Being able to break down 4-manfiolds in a consistent fashion into elementary pieces, while capturing the topological properties, makes them more accessible and allows for the generation of more complex examples.

Definition 2.2.1. [GK16] A $(g; k_1, k_2, k_3)$ -trisection of a smooth, closed, connected, oriented 4-manifold X^4 is a decomposition $X^4 = X_1 \cup X_2 \cup X_3$ with the following properties.

1. Each X_i is a 4-dimensional 1-handlebody, that is, diffeomorphic to $\natural^{k_i} S^1 \times B^3$. If $k_i = 0$, we interpret this boundary connected sum as B^4.

2. The X_i's intersect pairwise in genus g handlebodies (that is, their pairwise intersections are differomorphic to $H_g := \natural^g S^1 \times B^2$).

3. The triple intersection of the X_i's is a genus g oriented surface (denoted Σ_g), called the *central surface*.

If $k_1 = k_2 = k_3$, we call the trisection *balanced* and denote it as a $(g; k)$-trisection.

Figure 2.1 is a schematic depicting the decomposition of a 4-manifold into a trisection. The boundary for each X_i is the union of two genus g handlebodies, which is a Heegaard splitting for $\partial X_i \cong \partial(\natural^{k_i} S^1 \times S^2) = \sharp^{k_i} S^1 \times S^2$. The handlebodies H_i and the central surface

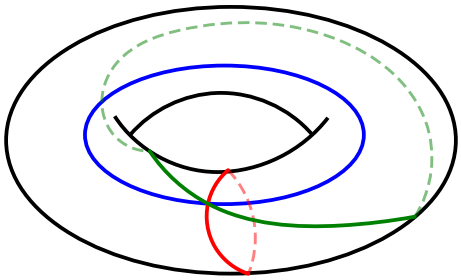

Figure 2.2: The standard (1;0) trisection diagram for $\mathbb{CP}^2$

make up the *spine* of the trisection. A trisection is uniquely determined by it's spine as there is a unique way, upto diffeomorphism, to fill this in with 4-dimensional 1-handlebodies [LP72].

Similar to Heegaard diagrams, trisection diagrams encode the information of the trisection using cut systems and the central surface.

Definition 2.2.2. [GK16] A $(g; k_1, k_2, k_3)$-*trisection diagram* is a surface along with three sets of pairwise disjoint simple closed curves $(\Sigma_g; \alpha, \beta, \gamma)$ such that $(\Sigma; \alpha, \beta)$, $(\Sigma; \beta, \gamma)$, and $(\Sigma; \gamma, \alpha)$ are diffeomorphic after handleslides to the standard Heegaard diagram for $\sharp^{k_i} S^1 \times S^2$.

Example $\mathbb{CP}^2$

$\mathbb{CP}^2$ admits the standard (1;0) trisection with the decomposition (up to diffeomorphism): $X_i = \mathbb{B}^4$, $H_i = \mathbb{S}^1 \times \mathbb{B}^2$ and $\Sigma = \mathbb{T}^2$. H_i pairwise gives us the Heegard splitting of $\partial\mathbb{B}^4 = \mathbb{S}^3$. The trisection diagram for $\mathbb{CP}^2$ is shown in Figure 2.2

2.2.2 Multisections

Islambouli and Naylor generalized trisections to multisections or n-sections, which is a decomposition into n pieces [IN20]. While every 4-manifold admits a trisection [GK16], cutting and regluing one of the pieces, never changes the manifold [LP72]. Multisections offer additional flexibility which allows cutting and re-gluing one of the pieces to change the manifold, giving us another way of thinking about 4-manifolds.

Definition 2.2.3. [IN20] Let X be a smooth, orientable, closed, connected 4-manifold. An *n-section, or multisection* of X is a decomposition $X = X_1 \cup X_2 \cup \cdots \cup X_n$ such that:

1. $X_i \cong \natural^{k_i} S^1 \times B^3$
2. $X_1 \cap X_2 \cap \cdots \cap X_n = \Sigma_g$, a closed orientable surface of genus g
3. $X_i \cap X_j = H_{i,j}$ is a 3-dimensional 1-handlebody if $|i-j| = 1$, and $X_i \cap X_j = \Sigma_g$ if $|i-j| > 1$
4. $\partial X_i \cong \sharp^{k_i} S^1 \times S^2$ has a Heegaard splitting given by $H_{(i-1),i} \cup_\Sigma H_{i,(i+1)}$.

Definition 2.2.4. [IN20] A *multisection diagram* is an ordered collection $(\Sigma; C_1, \ldots, C_n)$ where Σ is a surface, and $C_1, \ldots, C_n$ are cut systems for Σ, and each triple $(\Sigma; C_1, C_{i+1})$ is a Heegaard diagram for $\sharp^{k_i} S^1 \times S^2$ for some non-negative integer k_i (where the indices are taken mod n).

Example $\mathbb{CP}^1 \times \mathbb{CP}^1$

$\mathbb{CP}^1 \times \mathbb{CP}^1$ admits a genus 1 multisection with 4 sections (called a quadsection), as shown in Figure 2.3.

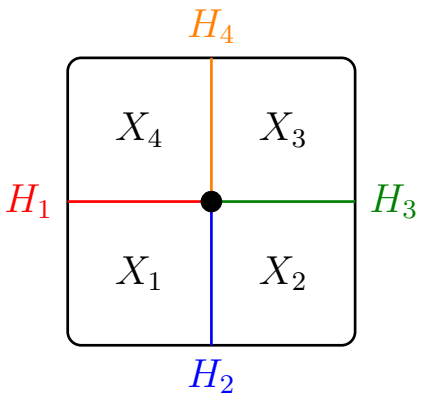

Figure 2.3: Genus 1 4-section of $\mathbb{CP}^1 \times \mathbb{CP}^1$

2.2.3 Relative Trisections

Castro, Gay and Pinzon-Caicedo defined relative trisections, which extended the notion of trisections to 4-manifolds with connected boundary [Cas+22].

For manifolds with boundary, each elementary piece X_i has a part of it's boundary which is going to form the boundary of the whole manifold $\partial_{out} X_i = X_i \cap \partial X$ and another which will glued to adjacent elementary pieces internally in the manifold $\partial_{in} X_i = X_i \cup X_j$. In fact, $\partial X = \cup \partial_{out} X_i$.

Instead of having a Heegaard decomposition with 3-dimensional handle bodies, we attach 3-dimensional 2-handles to get a generalized Heegaard splitting using compression bodies.

A *compression body* on Σ is a 3-manifold C obtained by attaching 3-dimensional 2-handles to a thickening of an orientable, connected surface with non-empty body Σ, i.e.

$$C = \Sigma \times [0,1] \cup \Sigma \times 1\{\text{3-dimensional 2-handles}\}$$

A *generalized Heegaard splitting* of M is a decomposition into compression bodies $V_i, W_i, i = 1, \ldots, n$ and surfaces $H_i, i = 1, \ldots, n$ such that $\partial_+ V_i = \partial_+ W_i = H_i$ and $\partial_- W_i = \partial_- V_{i+1}$. The interiors of the compression bodies must be pairwise disjoint and their union must be all of M. The surface H_i forms a Heegaard surface for the submanifold $V_i \cup W_i$ of M. (Note that here each V_i and W_i is allowed to have more than one component.)

For the sectors of the relative trisection, we define the following decomposition of the 4-dimensional 1-handlebody $Z = C \times [0,1]$ comping from the thickened compression body.

Consider the decomposition $\partial Z = \partial_{\text{in}} Z \cup \partial_{\text{out}} Z$, where

$$\partial_{\text{in}} Z = (C \times \{0\}) \cup (\partial_{-C} \times [0,1]) \cup (C \times \{1\}),$$

and

$$\partial_{\text{out}} Z = (\partial\Sigma \times [0,1] \times [0,1]) \cup (\partial_{+C} \times [0,1]).$$

The portion $\partial_{\text{in}} Z$ admits a (generalized) Heegaard splitting as $\partial_{\text{in}} Z = Y^- \cup Y^+$, where

$$Y^- = (C \times \{0\}) \cup (\partial_{-C} \times [0,1/2])$$

and

$$Y^+ = (\partial_{-C} \times [1/2,1]) \cup (C \times \{1\}).$$

In particular, the splitting surface is $Y^- \cap Y^+ = \partial_{-C} \times \{1/2\}$.

Definition 2.2.5. Let X be a smooth, oriented, and connected 4-manifold with connected non-empty boundary. A *relative trisection* $\mathcal{T}$ of X is a a decomposition $X = X_1 \cup X_2 \cup X_3$ such that:

- There are diffeomorphisms $\varphi_i : X_i \to Z$ such that $\varphi_i(X_i \cap \partial X) = \partial_{\text{out}} Z$,
- For each i, $\varphi_i(X_i \cap X_{i-1}) = Y^-$ and $\varphi_i(X_i \cap X_{i+1}) = Y^+$.

Definition 2.2.6. A $(g, k; p, b)$-relative trisection diagram is a tuple $(\Sigma; \alpha, \beta, \gamma)$, where Σ is a connected surface with non-empty boundary, α, β, γ are collections of disjoint embedded

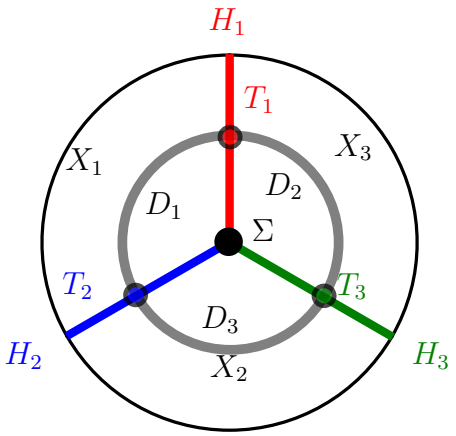

Figure 2.4: Schematic of a surface in bridge position with respect to the trisection

curves, and $(\Sigma;\alpha,\beta)$, $(\Sigma;\beta,\gamma)$, $(\Sigma;\gamma,\alpha)$ are slide-standard i.e. diffeomorphic to the standard diagram after handleslides.

2.3 Knotted Surfaces and Bridge Trisections

In 4-dimensions, the objects of interest are knotted surfaces, as all knots are trivial. Bridge trisections are decompositions of knotted surfaces in 4-dimensional manifolds, defined by Meir and Zupan [MZ18].

Given a trisection $\mathcal{T}$ splitting a 4-manifold X into $X_1 \cup X_2 \cup X_3$, we say that a knotted surface $S \subset X$ is in *bridge position* if $S \cap X_i$ is a collection of unknotted disks and $S \cap (X_i \cap X_j)$ is a collection of trivial tangles (See Figure 2.4). Any knotted surface S in X can be isotoped into bridge position with respect to $\mathcal{T}$ [MZ18].

Definition 2.3.1. [MZ18] A $(g;k_1,k_2,k_3;b;c_1,c_2,c_3)$-*bridge trisection* of a knotted surface S in a 4-manifold X is a decomposition $(X,S) = (X_1,D_1) \cup (X_2,D_2) \cup (X_3,D_3)$ with the following properties:

1. The decomposition $X = X_1 \cup X_2 \cup X_3$ is a $(g;k_1,k_2,k_3)$-trisection of X.
2. Each D_i is a boundary parallel collection of c_i disks in X_i.
3. The D_i's intersect pairwise in trivial b-strand tangles (denoted $T_\alpha, T_\beta, T_\gamma$) in the handlebodies which are the pairwise intersections of the X_i's.

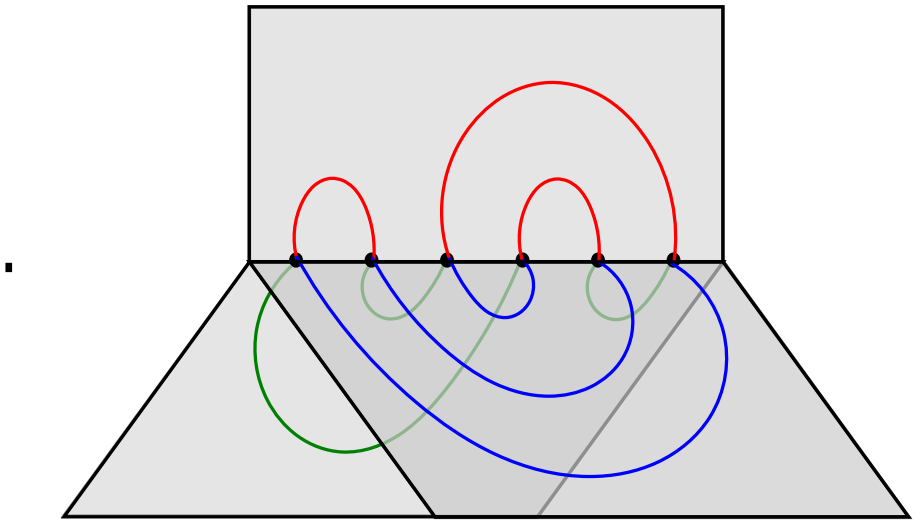

Figure 2.5: Triplane Diagram showcasing the shadow arcs for an unknotted torus $\mathbb{T}^2$.

Just as before, if $k_1 = k_2 = k_3 =: k$, we replace these parameters with just one k, and similarly for $c_1 = c_2 = c_3 =: c$.

Definition 2.3.2. A *shadow diagram* for a bridge trisection (X, S) is a triple $((\alpha, a), (\beta, b), (\gamma, c))$ of collections of curves and arcs in the central trisection surface Σ_g, where α, β, and γ are collections of trisection diagram curves for X, and a, b, and c are collections of *shadow arcs*, i.e. projections onto the central surface (See Figure 2.5), for the trivial tangles T_α, T_β, and T_γ, respectively.

Chapter 3

Moduli Spaces of Lagrangian Surfaces in $\mathbb{CP}^2$ obtained from Triple Grid Diagrams

3.1 Triple grid diagrams and Lagrangian surfaces

One geometric motivation to study triple grid diagrams is that they determine Lagrangian surfaces in $\mathbb{CP}^2$. A triple grid diagram D determines three standard grid diagrams $\mathbb{G}_1, \mathbb{G}_2, \mathbb{G}_3$. Via a well-known method, grid diagrams determine Legendrian links in the standard tight contact structure (S^3, ξ_{std}).

Start with $(\mathbb{CP}^2, \omega_{FS})$ and remove three Darboux balls. The result is a symplectic 4-manifold (X, ω) with three boundary components Y_1, Y_2, Y_3, each with an inward-pointing Liouville vector field ρ_i. The 1-form $\alpha_i = \omega(\rho_i, -)$ is a contact form for the standard tight contact structure ξ_{std} on S^3. This symplectic 4-manifold is a *strong symplectic cap* for the disjoint union of three copies of (S^3, ξ_{std}). A *Lagrangian cap* is a surface L that intersects the boundary transversely, such that $\omega|_L = 0$ and each Liouville vector field ρ_i is tangent to L in some neighborhood of the boundary. Consequently, the link $\Lambda_i = L \pitchfork Y_i$ is a Legendrian link tangent to the contact structure ξ_{std} along Y_i.

Theorem 3.1.1 ([BGL23])**.** *A geometric triple grid diagram D determines a Lagrangian cap $L(D)$ in (X, ω) for the three disjoint Legendrian links $\Lambda_1, \Lambda_2, \Lambda_3$ determined by the three induced grid diagrams.*

Furthermore, if each Λ_i admits a Lagrangian filling in (B^4, ω_{std}), then these fillings can be glued to the Lagrangian cap $L(D)$ to produce an embedded Lagrangian surface.

3.1.1 Fillability obstructions

A triple grid diagram D determines a Lagrangian cap $L(D)$ in $(CP^2 \setminus 3B^4, \omega)$ for a triple $\Lambda_{\alpha\beta} \cup \Lambda_{\beta\gamma} \cup \Lambda_{\gamma\alpha}$ of Legendrian links. If each Legendrian link admits a Lagrangian filling in (B^4, ω_{std}), then these fillings can be glued to the Lagrangian cap to obtain an embedded, Lagrangian surface in $\mathbb{CP}^2$. Suppose that each Legendrian link admits a Lagrangian filling by disks. The Euler characteristic and orientability of the resulting closed surface $L(D)$ is determined by the abstract, Tait-colored cubic graph Γ.

The torus $\mathbb{T}^2$ is the only orientable surface that admits a Lagrangian embedding in $\mathbb{CP}^2$. For nonorientable surfaces, the real projective plane (realized as the set of real points in $\mathbb{CP}^2$) is Lagrangian, but Shevchishin [She09] and Nemirovski [Nem09] showed that the Klein bottle does not admit a Lagrangian embedding. Furthermore, the combined work of Givental [Giv86], Audin [Aud90], and Dai, Ho, and Li [DHL19] establishes that $\#^k\mathbb{RP}^2$ admits a Lagrangian embedding into $\mathbb{CP}^2$ if and only if $k \equiv 2 \pmod 4$ and $k \neq 2$ or if $k \equiv 1 \pmod 4$.

Therefore, we can obstruct the existence of Lagrangian fillings by the following method. Take an abstract, Tait-colored cubic graph Γ that determines a nonorientable surface with nonpositive Euler characteristic either identically 0 or equal to $2, 3 \pmod 4$. Construct the moduli of triple grid diagrams modeled on Γ and consider a given triple grid diagram D. If at least two of the resulting Legendrian links admit Lagrangian fillings by disks, then the third Legendrian link cannot.

3.1.2 Extension to almost-toric fibrations

A *Markov triple* is a solution (a, b, c) to the Diophantine equation

$$a^2 + b^2 + c^2 = 3abc$$

The base example is $(1, 1, 1)$ and any other Markov triple can be obtained through a sequence of 'mutations'.

Given a Markov triple, the toric structure on the weighted projective plane $\mathbb{CP}^2(a^2, b^2, c^2)$ can be deformed to an almost-toric structure. Vianna [Via16], for example, showed that the central fiber $T_{a,b,c}$ of such an almost-toric fibration is an exotic monotone Lagrangian torus. This torus bounds three solid tori $S^1 \times \mathbb{D}^2$ corresponding to three compressing slopes $\alpha, \beta, \gamma \in H_1(T^2)$ satisfying the modified cocycle equation

$$a^2\alpha + b^2\beta + c^2\gamma = 0$$

A neighborhood of the union $\mathcal{S} = H_\alpha \cup H_\beta \cup H_\gamma$ admits a symplectic structure with three strongly concave boundary components. Each is a lens space with a universally tight contact structure that can be symplectically filled with a rational homology 4-ball. Although not stated explicitly in [BGL23], Theorem 3.1.1 can be immediately extended to triple grid diagrams defined with respect to a triple of slopes (α, β, γ) defined by a Markov triple. It may therefore be interesting to study fillable triple grid diagrams with respect to all such slope triples and almost-toric fibrations of $\mathbb{CP}^2$. We remark that in our method for computing the moduli space $\mathcal{M}(\Gamma)$ can be immediately adapted to compute the moduli spaces with respect to any slope triple.

3.2 Main Theorem

We give an elegant geometric construction that produces all triple grid diagrams. The insight is to conduct the search by conditioning on the abstract, Tait-colored cubic graph Γ one is trying to realize by a triple grid diagram, as oppposed to conditioning on the grid size n. From this perspective, the problem is purely linear algebra and can be solved quickly in polynomial time; whereas testing pairs of permutations requires $O((n!)^2)$-time. In fact, we can prove the existence of triple grid diagrams purely by counting dimensions of intersecting linear subspaces. This is joint work with Lambert-Cole [GL24].

Theorem 3.2.1. *Let Γ be an abstract Tait-colored cubic graph with $2b$ vertices. The moduli space $\mathcal{M}(\Gamma)$ of geometric triple grid diagrams with graph-type Γ is a smooth manifold.*

1. *If $b = 1$, then the moduli space is empty.*
2. *If $b = 2$, then the moduli space is 2-dimensional and consists of $\mathbb{T}^2$-translates of a single element, the $\mathbb{RP}^2$-graph in Figure 3.4.*
3. *If $b \geq 3$, then $\mathcal{M}(\Gamma)$ is nonempty and has dimension $d \geq b$.*

This theorem is a combination of Theorem 3.4.1 and Examples 3.5.1 and 3.5.2.

3.3 Terminology and Definitions

3.3.1 Triple Grid Diagrams

Definition 3.3.1. A *grid diagram* comprises a $n \times n$ grid on a torus with the restriction that each row and column between the grid lines has exactly zero dots or two dots.

Definition 3.3.2. A *Triple Grid (combinatorial) diagram* $\mathcal{D}(n, b)$ is a grid diagram of size n with additional information. It consists of the following :

1. a grid on the torus $T^2 = \mathbb{R}^2/\mathbb{Z}^2$ consisting of three sets of lines:
   (a) n vertical lines $\left\{x = \frac{k}{n} : 1 \leq k \leq n\right\}$, colored red by convention,
   (b) n horizontal lines $\left\{y = \frac{k}{n} : 1 \leq k \leq n\right\}$, colored blue by convention, and
   (c) n diagonal lines (of slope -1) $\left\{x + y = \frac{k}{n} : 1 \leq k \leq n\right\}$, colored green by convention.
2. $2b$ points in the complement of the $3n$ grid lines, such that in the region between any pair of adjacent lines of the same slope, there are exactly zero or two points.

It can be decomposed into three grid diagrams of size b each. See Figure 3.1 for an example.

Definition 3.3.3. A Triple Grid diagram of size b is said to be *orientable* if there exists a partition of the $2b$ points into b Xs and b Os such that each vertical line, a horizontal line, and diagonal line has one X and one O.

Lemma 3.3.4. *A Triple Grid diagram being orientable is equivalent to the corresponding cubic Tait-colored graph being bipartite.*

Proof. The proof is by definition. If Γ is bipartite, then we can label the vertices in one partition by Xs and the other by Os. As Γ is cubic and Tait-colored, every (red, blue, or green) edge joins an X to an O. So, in the corresponding Triple Grid diagrams, this corresponds to 2 points on a line (horizontal, vertical, or diagonal respectively) with one being labeled with X and the other with O i.e. being orientable. Let $\mathcal{D}$ be an orientable Triple grid diagram. Then we can obtain Γ by connecting points with colored edges and forgetting the torus. Since each edge connects an X with an O, Γ is partitioned into Xs and Os. □

Note that we are allowing empty rows and columns, unlike those in grid homology. This is because empty rows and columns do not change the link in the grid diagram and are needed to satisfy the diagonal condition in the corresponding Triple grid diagram.

3.3.2 Geometric Triple Grid Diagrams

In order to determine whether a grid diagram satisfies the conditions for being a Triple grid diagram, we assume that it is a Triple grid diagram and proceeds to verify that each of the encoded grid diagrams satisfies the relevant restrictions.

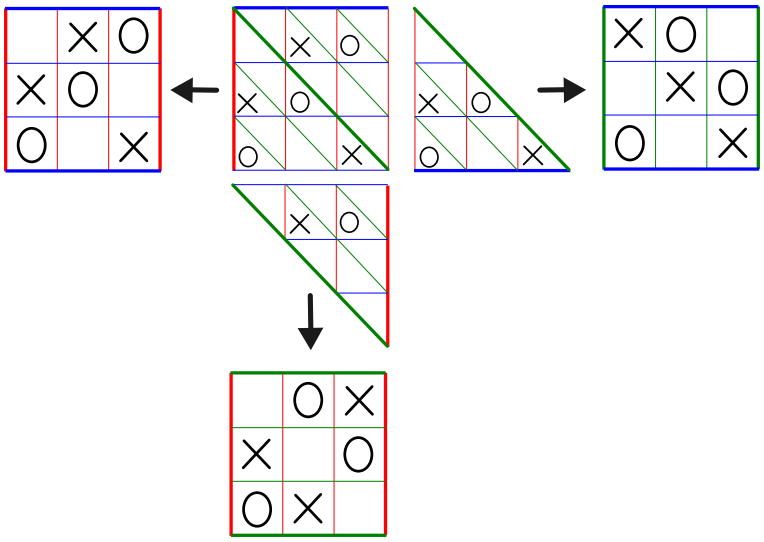

Figure 3.1: The Triple Grid diagram corresponding to $K_{3,3}$ and the three Grid diagrams it encodes. The upper and lower triangles of the Triple Grid diagram have been repeated to show how to obtain the encoded Grid diagrams.

This method of searching for combinatorial Triple Grid diagrams of orientable grid number and size n has a complexity of $O((n!)^2)$ since it requires iterating through all possible grid diagrams. As such, we were only able to enumerate all possible Triple grid diagrams up to a size of $n = 9$. Moreover, the output Triple Grids have symmetry coming from translations, swapping of grids, and swapping of colors. This resulted in a lot of repetition in the output. Further, trying to narrow down the output to fillable Triple Grid diagrams was difficult as the output was the order of hundreds of diagrams.

In light of these challenges, we propose an alternative approach for investigating Triple grid diagrams. Specifically, we fix a cubic Tait-colored graph Γ and consider all maps of the vertex set $V(\Gamma)$ into $\mathbb{T}^2$. This approach not only provides a more efficient means of studying the moduli space of Triple grid diagrams but also allows for the definition of Triple Grid moves. We are also able to search fillable Triple Grid diagrams more systematically.

Definition 3.3.5. A *cubic (abstract) graph* $\Gamma = (V, E)$ is a graph such that each vertex has degree 3 i.e. 3 edges. A *cubic graph* is said to be *Tait-colored* if we can assign a color (red, blue, or green) to each edge of the graph in such a way that at each vertex, the 3 edges incident to that vertex is colored with exactly three distinct colors.

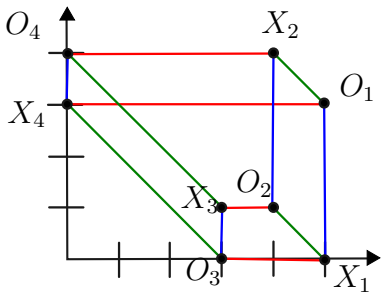

Figure 3.2: Geometric Triple Grid diagram of Torus with $b = 4$.

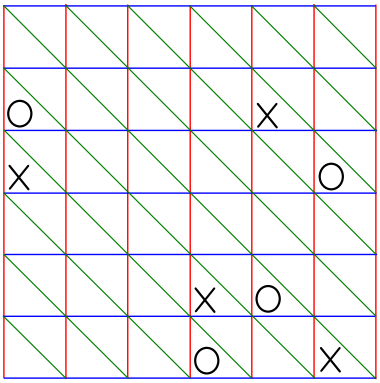

Figure 3.3: Combinatorial Triple Grid diagram of Torus with $b = 4$.

We can define Triple Grid graphs as immersions of Tait-colored cubic graphs into the central torus of $\mathbb{CP}^2$. As we are looking at these graphs from the viewpoint of surfaces, we need them to be well-defined. Therefore, we can not allow double points and overlaps on the central torus. Note that since each point on the central torus has coordinates, this is equivalent to a Geometric Triple Grid diagram.

Definition 3.3.6. Let $\phi : \Gamma \longrightarrow \mathbb{T}^2 = \mathbb{R}^2/\mathbb{Z}^2$ such that

1. $\phi(v_i) = \phi(v_j)$ if and only if $i = j$.

   2. a) $x_i = x_j$ if and only if $e_{(i,j)} \in E_{red}$.

   2. b) $y_i = y_j$ if and only if $e_{(i,j)} \in E_{blue}$.

   2. c) $x_i + y_i = x_j + y_j$ if and only if $e_{(i,j)} \in E_{green}$.

Then $\phi(\Gamma)$ defines a Triple Grid diagram.

Definition 3.3.7. The *Geometric Triple Grid diagram* Θ consists of $2b$ points(vertices/dots) in $\mathbb{T}^2 = \mathbb{R}^2/\mathbb{Z}^2$. These points $(x_i, y_i)_1^{2b}$ satisfy the following conditions:

- For each line $x = c$, either there are either exactly two points on it or none.
- For each $y = c$, either there are either exactly two points on it or none.
- For each line $x + y = c$, either there are either exactly two points on it or none.

The Triple Grid can be decomposed into three Grid Diagrams by thinking of a third coordinate $z = -x - y$. Then looking at (x, y),(y, z), and (z, x) gives us the Grid diagrams making up the Triple Grid diagram.

Definition 3.3.8. The *Geometric Grid diagram* consists of $2b$ points(vertices/dots) in $\mathbb{T}^2 = \mathbb{R}^2/\mathbb{Z}^2$. These points $(x_i, y_i)_1^{2b}$ satisfy the following conditions:

- For each line $x = c$, either there are either exactly two points on it or none.
- For each $y = c$, either there are either exactly two points on it or none.

3.4 Moduli Space of Geometric Triple Grids

Let $\Gamma = (V, E)$ be a cubic Tait-colored graph. Define

$$I(\Gamma) := \left\{\phi : V(\Gamma) \to \mathbb{T}^2\right\} \cong (\mathbb{T}^2)^{2b}$$

to be the set of maps of the vertex set $V(\Gamma)$ into $\mathbb{T}^2$. We can then realize the moduli space of triple grid diagrams with 1-skeleton Γ as a subspace of $I(\Gamma)$. In particular,

$$\mathcal{M}(\Gamma) := \left\{ \phi : V(\Gamma) \longrightarrow \mathbb{T}^2 \;\middle|\; \begin{array}{cc} x_i = x_j & \text{if and only if } e_{(i,j)} \in E_{red}, \\ y_i = y_j & \text{if and only if } e_{(i,j)} \in E_{blue}, \\ x_i + y_i = x_j + y_j & \text{if and only if } e_{(i,j)} \in E_{green} \end{array} \right\}$$

The main result of this section is that this moduli space is nonempty if the vertex set is sufficiently large.

Theorem 3.4.1. *Let Γ be a Tait-colored cubic graph with $2b$ vertices. The moduli space $\mathcal{M}(\Gamma)$ of geometric triple grid diagrams with graph-type Γ is a smooth manifold of dimension greater than or equal to b.*

To prove this theorem, we adopt a more 'linear' perspective and alternately describe $I(\Gamma)$ and $\mathcal{M}(\Gamma)$ in terms of $\mathbb{T}^2$-valued cochains on Γ. We first identify $I(\Gamma)$ with a subspace of $C^*(\Gamma, \mathbb{T}^2)$. The slope restrictions on the edges can be expressed in terms of a linear subspace $S \subset C^1(\Gamma, \mathbb{T}^2)$ and the nondegeneracy conditions on the vertices can be expressed in terms of a union of hyperplanes $D \subset C^0(\Gamma, \mathbb{T}^2)$. Then $\mathcal{M}(\Gamma)$ corresponds to the subset of $I(\Gamma)$ contained in S but in the complement of D.

3.4.1 The space $\mathrm{I}(\Gamma)$

Lemma 3.4.2. *There are identifications*

$$\mathrm{I}(\Gamma) = C^0(\Gamma, \mathbb{T}^2) = \ker d^* \bigoplus \mathrm{Im}\, d^* \subset C^0(\Gamma, \mathbb{T}^2) \times C^1(\Gamma, \mathbb{T}^2)$$

Proof. Let $\phi \in \mathrm{I}(\Gamma)$ be a map. It assigns a point in $\mathbb{T}^2$ to each vertex

$$\phi(v_i) = \vec{x_i} \in \mathbb{T}^2$$

On the other hand, a 0-cochain in $C^0(\Gamma, \mathbb{T}^2)$ is by definition a homomorphism $\tilde{X} : C_0(\Gamma, \mathbb{T}^2) \longrightarrow \mathbb{T}^2$. Let $x_0 \in \mathbb{T}^2$ be a fixed basepoint. Then there is a basis for $C_0(\Gamma, \mathbb{T}^2)$ consisting of the 0-chains that assigns x_0 to each vertex. Consequently, we can identify the map ϕ with the 0-cochain that sends the v_i 0-chain to $\phi(v_i) \in \mathbb{T}^2$.

The second identification is given by the first isomorphism theorem for linear maps. Explicitly, we can identify ϕ with a pair (X, W) such that

$$\begin{aligned} X : \{v_i\} &\longrightarrow \mathbb{T}^2 & \qquad W : \{e_{ij}\} &\longrightarrow \mathbb{T}^2 \\ X(v_i) &= \vec{x_i} & \qquad W(e_{ij}) &= \vec{x_j} - \vec{x_i} \end{aligned}$$

□

The kernel of d^* is precisely the constant 0-cochains and can be identified with $\mathbb{T}^2$. Geomtrically, this summand correponds to translations of ϕ in $\mathbb{T}^2$. Passing to homology, we have the diagram

$$\begin{array}{ccccc} C^0(\Gamma, \mathbb{T}^2) & \xrightarrow{d^*} & C^1(\Gamma, \mathbb{T}^2) & \longrightarrow & 0 \\ & & \downarrow{\scriptstyle i^*} & & \\ & & H^1(\Gamma, \mathbb{T}^2) & & \end{array}$$

and exactness implies that $\operatorname{Im} d^* = \ker i^*$.

Corollary 3.4.3. *There is an identification*

$$\mathrm{I}(\Gamma) = \mathbb{T}^2 \oplus \ker i^*$$

Denote $I_0(\Gamma) := \operatorname{Im} d^* \cong \ker i^*$.

3.4.2 Slope Restrictions

The slope restrictions on a triple grid diagram can be reinterpreted in terms of a linear subspace in $C^1(\Gamma, \mathbb{T}^2)$.

The restriction on the coordinates that $x_i = x_j$ if $e_{(i,j)} \in E_{red}$ can be rephrased as $W(e_{ij}) = \vec{x_j} - \vec{x_i} \in (\mathbb{S}^1 \times 0) \subset \mathbb{T}^2$, if $e_{(i,j)} \in E_{red}$. This is a hyperplane in $C^1(\Gamma, \mathbb{T}^2)$. Repeating this for each edge, the slope restraints arising from the coloring correspond to restricting to a subset S of $C^1(\Gamma, \mathbb{T}^2)$ that is the common intersection of multiple hyperplanes.

$$S := \left\{ W : C_1(\Gamma, \mathbb{T}^2) \longrightarrow \mathbb{T}^2 \;\middle|\; \begin{array}{llll} W(e_{ij}) & = \vec{x_j} - \vec{x_i} & \in (\mathbb{S}^1 \times 0) & \text{if } e_{(i,j)} \in E_{red} \\ W(e_{ij}) & = \vec{x_j} - \vec{x_i} & \in (0 \times \mathbb{S}^1) & \text{if } e_{(i,j)} \in E_{blue} \\ W(e_{ij}) & = \vec{x_j} - \vec{x_i} & \in \Delta = \{(x,x) \in \mathbb{T}^2\} & \text{if } e_{(i,j)} \in E_{green} \end{array} \right\}$$

Let $\mathcal{M}_0(\Gamma)$ denote *based* Geometric Triple Grid diagrams, where a designated vertex v_1 is mapped to a distinguished basepoint $(0,0)$ in $\mathbb{T}^2$:

$$\mathcal{M}_0(\Gamma) := \left\{ \phi : \Gamma \longrightarrow \mathbb{T}^2 \;\middle|\; \begin{array}{ll} x_i = x_j & \text{if } e_{(i,j)} \in E_{red}, \\ y_i = y_j & \text{if } e_{(i,j)} \in E_{blue}, \\ x_i + y_i = x_j + y_j & \text{if } e_{(i,j)} \in E_{green}, \\ \phi(v_1) = (0,0) & \end{array} \right\}$$

Then

Lemma 3.4.4. *There is an inclusion*

$$\mathcal{M}(\Gamma) \subset (\ker d^*) \oplus (\operatorname{Im} d^* \cap S) \cong \mathbb{T}^2 \oplus I_0(\Gamma)$$

Moreover, the dimension of moduli of based Geometric Triple Grid diagrams satisfies

$$\dim \mathcal{M}_0(\Gamma) \geq b - 2$$

Proof. The inclusion is true by construction.

The dimension of $I(\Gamma)$ is given by

$$\dim(\mathrm{I}(\Gamma)) = \dim(C^0(\Gamma, \mathbb{T}^2)) = |V| \times \dim(\mathbb{T}^2) = 2b \times 2 = 4b$$

and $\dim \operatorname{Im} d^* = \dim(\mathrm{I}(\Gamma)) - 2$. The dimension of S is exactly half the dimension of $C^1(\Gamma, \mathbb{T}^2)$, since each 1-cochain is constrained to lie in a 1-dimensional subspace of $\mathbb{T}^2$. Therefore

$$\dim S = \frac{1}{2} \dim C^1(\Gamma, \mathbb{T}^2) = \frac{1}{2}(|E| \times 2) = |E| = 3b$$

Combining this, we have

$$\dim(\operatorname{Im} d^* \cap S) \geq \dim \operatorname{Im} d^* + \dim S - \dim C^1(\Gamma, \mathbb{T}^2) = 4b - 2 + 3b - 6b = b - 2$$

So, $\dim(\operatorname{Im} d^* \cap S) = \dim \mathcal{M}_0(\Gamma) \geq b - 2$.

□

3.4.3 Degenerate Immersions

Similarly, the nondegeneracy conditions on a triple grid diagram can be reinterpreted in terms of the complement of a hyperplane arrangement in $C^0(\Gamma, \mathbb{T}^2)$.

To ensure that $x_i = x_j$ only if $e_{(i,j)} \in E_{red}$, we need to remove the cases when $x_i = x_k$ for $e_{(i,k)} \notin E_{red}$. Let $\tilde{X} \in C^0(\Gamma, \mathbb{T}^2)$. Then

$$\begin{aligned} \tilde{X} : C_0(\Gamma, \mathbb{T}^2) &\longrightarrow \mathbb{T}^2 \\ v_i &\longmapsto (x_i, y_i) \end{aligned}$$

Define

$$R_{i,k} := \left\{ \tilde{X} : x_i = x_k \right\}$$

It is a codimension-1 hyperplane in $C^0(\Gamma, \mathbb{T}^2)$. Let $\mathcal{R}_{i,k} = R_{i,k} \oplus C^1(\Gamma, \mathbb{T}^2)$ and

$$\mathcal{R} = \bigcup_{\substack{i,k \\ e_{i,k} \notin E_{red}}} \mathcal{R}_{i,k}$$

Define $B_{i,k}, \mathcal{B}$ and $G_{i,k}, \mathcal{G}$ similarly for the blue and green edges, respectively. Then $D = \mathcal{R} \cup \mathcal{B} \cup \mathcal{G}$ is a union of hyperplanes in $C^*(\Gamma, \mathbb{T}^2)$ and a triple grid diagram must lie in the complement of D.

This gives us the following proposition.

Proposition 3.4.5.

$$\mathcal{M}(\Gamma) = \big((\ker d^*) \oplus (\operatorname{Im} d^* \cap S)\big) \setminus D = \big((\mathbb{T}^2) \oplus \mathcal{M}_0(\Gamma)\big) \setminus D$$

Since D has codimension 1, removing it does not affect the dimension. Then Theorem 3.4.1 follows from the above proposition and Lemma 3.4.4.

3.5 Examples

Example 3.5.1. Let us consider the case when $b = 1$. Then the only cubic Tait colored graph possible is the theta graph. Since the two vertices are connected by edges of all three colors, the immersion needs to connect two points with lines having slope 0, 1 and ∞. The only immersion possible is degenerate.

Example 3.5.2. There is only one cubic Tait colored graph having $b = 2$, which is shown in Figure 3.4a. This graph represents $\mathbb{RP}2$. From Proposition 4.5, $\dim \mathcal{M}(\Gamma) \geq 2$ and $\dim \mathcal{M}_0(\Gamma) \geq 0$. Due to the slope restritions, there is only one Geometric Triple Grid diagram upto translation, shown in Figure 3.4b. Hence these inequalities are strict for $\mathbb{RP}2$.

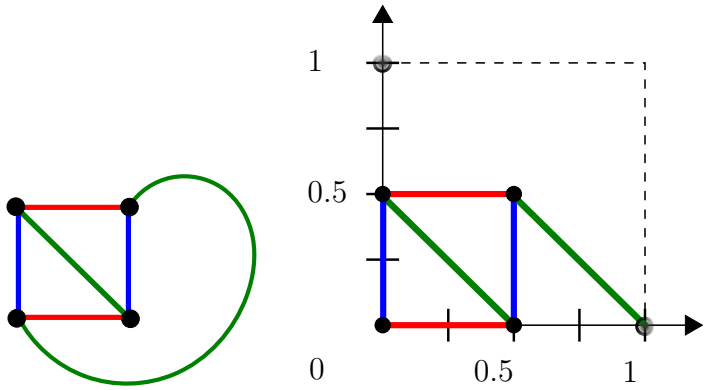

(a) Γ with $b = 2$ (b) Geometric Triple Grid Diagram

Figure 3.4: Example with $b = 2$ representing $\mathbb{RP}2$

Example 3.5.3. Consider Γ to be the graph $K_{3,3}$, having $b = 3$. This symmetric graph has only Tait-coloring possible depicted in Figure 3.5a. Due to Theorem 3.2.1,we know that $\dim \mathcal{M}(K_{3,3}) \geq 3$ and $\dim \mathcal{M}_0(K_{3,3}) \geq 1$. By calculation, we see that $\mathcal{M}'(K_{3,3}) \cong \mathbb{T}^2$ represented in Figure 3.5c, and so $\dim \mathcal{M}(K_{3,3}) = 4$.

The pink line in the center is a plane in D, which denotes degenerate immersions of $K_{3,3}$, along with the lines $p_1 = 0$ and $p_2 = 0$ The yellow region and the cyan blue region correspond to two regions in $\mathcal{M}'(K_{3,3})$. Each region maps to Geometric Triple Grid diagrams which differ by minor perturbations and therefore correspond to the same Triple Grid diagram. Going from one Triple Grid diagram to another requires passing through a hyperplane in D. Therefore, Triple Grid moves can be defined as moving through a degenerate immersion. These moves do not change the underlying graph Γ and therefore so not change the surface in the bridge trisection.

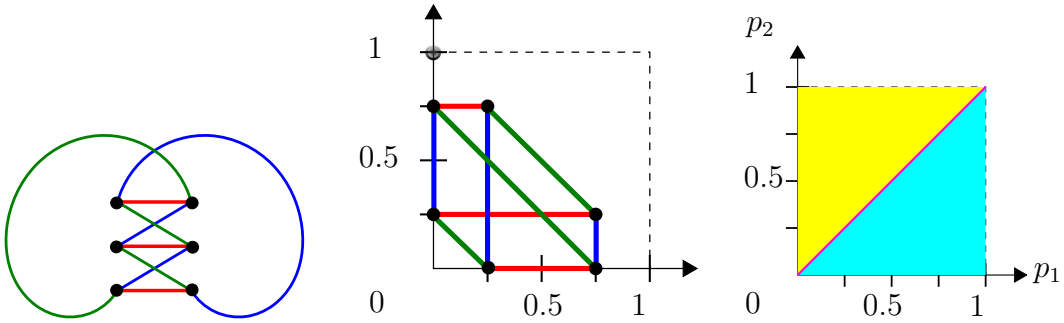

(a) Γ with $b = 3$ (b) Geometric Triple Grid (c) Moduli Space

Figure 3.5: Example Graph $K_{3,3}$ with $b = 3$ representing

Example 3.5.4. For $b = 4$, consider Γ to be the cubic Tait-colored graph in Figure 3.7a which corresponds to $\mathbb{T}^2$. Due to Theorem 3.2.1, we know that $\dim \mathcal{M}(\Gamma) \geq 4$ and therefore $\mathcal{M}_0(\Gamma) \geq 2$.

By calculation, we get that $\mathcal{M}_0(\Gamma) \cong \mathbb{T}^3$ as shown in Figure 3.7b. The moduli space is divided in to 6 regions by 6 degenerate planes, which correspond to $p_1 = 0$,$p_2 = 0$,$p_3 = 0$, $p_1 = p_2$, $p_2 = p_3$, $p_3 = p_1$ in this parameterized representation. We can see Geometric Triple Grid Diagrams from each of the 6 differently colored regions, represented in Figure 3.6a. These give us the corresponding Combinatorial Triple Grid Diagrams, as shown in Figure 3.6b. Therefore, by fixing the underlying graph Γ, we are able to find all the equivalent Triple Grid Diagrams. We can also see many Triple Grid moves, like the one shown in Figure 3.8.

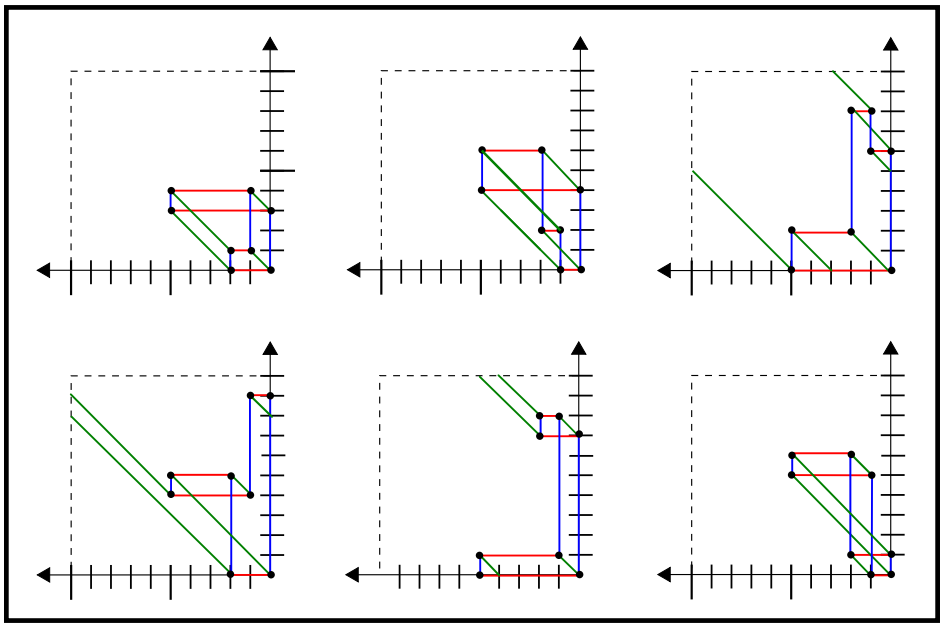

(a) Six Geometric Triple Grid diagrams corresponding to the six regions in the moduli space for the $b = 4$ example in Figure 3.7

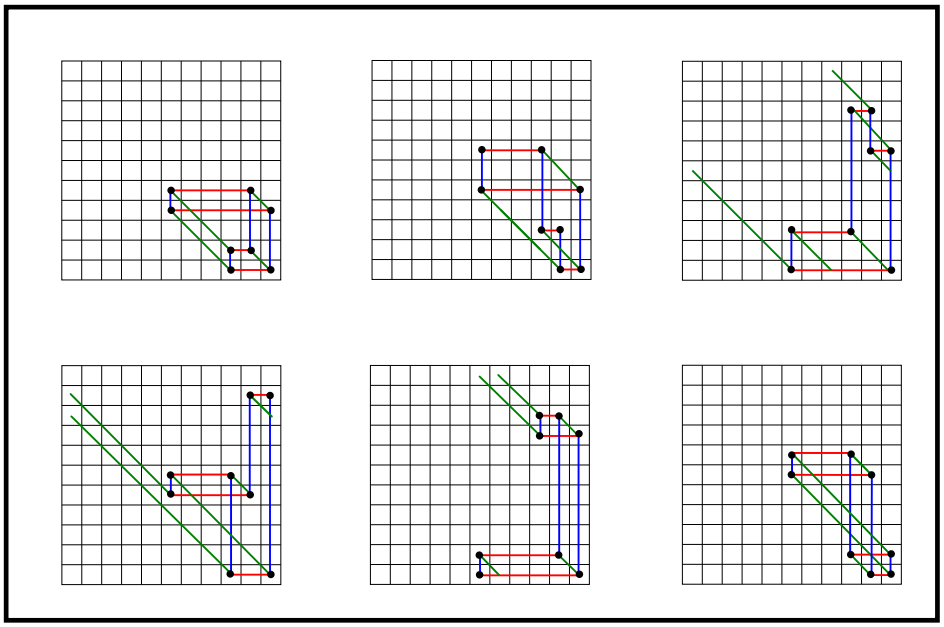

(b) Six **Combinatorial** Triple Grid diagrams corresponding to the six regions in the moduli space for the $b = 4$ example

Figure 3.6: Triple Grid diagrams for the regions in the moduli space for the $b = 4$

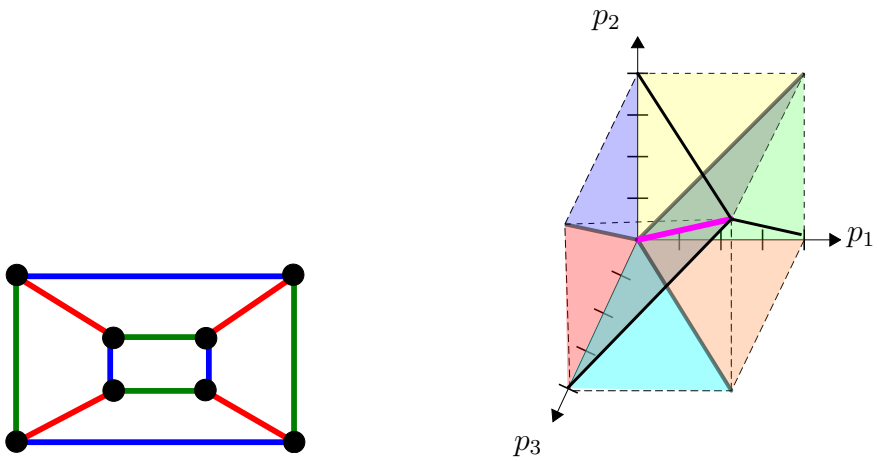

(a) Γ with $b = 4$ (b) Moduli Space

Figure 3.7: Example with $b = 4$ representing $\mathbb{T}^2$

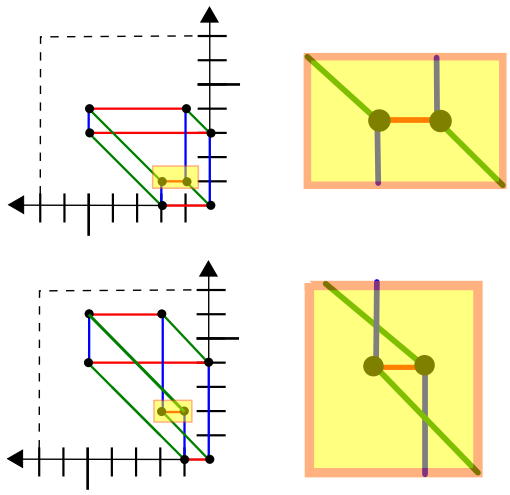

Figure 3.8: Example of Triple Grid Move

Note that the degenerate planes $p_1 = p_2$, $p_2 = p_3$ and $p_3 = p_1$ intersect at the line $p_1 = p_2 = p_3$ represented in pink in the figure. Therefore, we can see that all 6 regions share this line in their boundary.

3.6 Computation

Cochains with $\mathbb{T}^2$-coefficients are computationally awkward. Instead, we can use the fact that $\mathbb{T}^2 = \mathbb{R}^2/\mathbb{Z}^2$ and work with $\mathbb{R}^2$-valued cochains instead. The moduli $\mathcal{M}(\Gamma)$ of triple grid diagrams can be modeled as a *subset* of $C^0(\Gamma, \mathbb{T}^2)$, but a suitable cover of $\mathcal{M}(\Gamma)$ can be realized as a collection of affine subspaces in $C^1(\Gamma, \mathbb{R}^2)$. In particular, these are solution sets to systems of linear equations and can therefore be computed in polynomial time.

From the short exact sequence

$$0 \to \mathbb{Z}^2 \to \mathbb{R}^2 \to \mathbb{T}^2 \to 0$$

we obtain a short exact sequence of cochain complexes

$$\begin{array}{ccccccccc}
 & & 0 & & 0 & & 0 & & \\
 & & \uparrow & & \uparrow & & \uparrow & & \\
0 & \longrightarrow & C^1(\Gamma, \mathbb{Z}^2) & \xhookrightarrow{d_s^*} & C^1(\Gamma, \mathbb{R}^2) & \xrightarrow{d_r^*} & C^1(\Gamma, \mathbb{T}^2) & \longrightarrow & 0 \\
 & & \uparrow d^* & & \uparrow d* & & \uparrow d^* & & \\
0 & \longrightarrow & C^0(\Gamma, \mathbb{Z}^2) & \xhookrightarrow{d_s^*} & C^0(\Gamma, \mathbb{R}^2) & \xrightarrow{d_r^*} & C^0(\Gamma, \mathbb{T}^2) & \longrightarrow & 0
\end{array}$$

We identify $I(\Gamma)/\mathbb{T}^2$ with the subspace of coexact cochains in $C^1(\Gamma, \mathbb{T}^2)$. Via the short exact sequence of chain complexes, we can lift every 1-cochain in $C^1(\Gamma, \mathbb{T}^2)$ to a 1-cochain in $C^1(\Gamma, \mathbb{R}^2)$. Since the diagram is commutative, it follows that every exact 1-cochain $\mathbf{x}$ in $C^1(\Gamma, \mathbb{T}^2)$ lifts to an exact 1-cochain $\widetilde{\mathbf{x}}$ in $C^1(\Gamma, \mathbb{R}^2)$. The slope conditions $S \subset C^1(\Gamma, \mathbb{T}^2)$ also lifts to a linear subspace $\widetilde{S}$ in $C^1(\Gamma, \mathbb{R}^2)$ that contains the origin.

However, it does not follow that $\mathbf{x}$ satisfies the slope condition S only if the lift $\widetilde{\mathbf{x}}$ lies in the subspace $\widetilde{S}$. The preimage of $I(\Gamma)$ in $C^1(\Gamma, \mathbb{R}^2)$ is strictly larger than the subspace of coexact 1-cochains in $C^1(\Gamma, \mathbb{R}^2)$. From the short exact sequence of complexes, we obtain a surjection

$$C^1(\Gamma, \mathbb{Z}^2) + \mathrm{Im}(d^0_{\mathbb{R}}) \longrightarrow \mathrm{Im}(d^0_{\mathbb{T}^2}) \subset C^1(\Gamma, \mathbb{T}^2)$$

In fact, we can strengthen this to a surjection

$$\mathrm{Coker}(d^0_{\mathbb{Z}}) \oplus \mathrm{Im}(d^0_{\mathbb{R}}) \to \mathrm{Im}(d^0_{\mathbb{T}^2})$$

since $\mathrm{Im}(d^0_{\mathbb{Z}})$ injects into $\mathrm{Im}(d^0_{\mathbb{R}})$. Finally, we can identify $\mathrm{Coker}(d^0_{\mathbb{Z}})$ with $H^1(\Gamma, \mathbb{Z}^2)$. Summarizing this discussion, we have the following proposition.

Proposition 3.6.1. *Let $\mathbf{x} \in C^1(\Gamma, \mathbb{T}^2)$ be an exact 1-cocycle. Then $\mathbf{x}$ satisfies the slope condition S if and only if there exists a lift $\widetilde{\mathbf{x}} \in Im(d^0_{\mathbb{R}})$ and a class $\rho \in H^1(\Gamma, \mathbb{Z}^2) \cong Coker(d^0_{\mathbb{Z}}) \cong Im(d^0_{\mathbb{Z}})^\perp$ such that*

$$\widetilde{\mathbf{x}} + \rho \in \widetilde{S}$$

Moreover, the lift $\widetilde{\mathbf{x}}$ is unique up to an element $\widetilde{\mathbf{y}} \in \widetilde{S} \cap Im(d^0_{\mathbb{Z}})$ and ρ is unique up to an element of $Im(d^0_{\mathbb{Z}})^\perp \cap \widetilde{S}$.

This proposition implies that we can decompose $\mathcal{M}(\Gamma)$ into components $\mathcal{M}_\rho(\Gamma)$, indexed by elements $\rho \in H^1(\Gamma, \mathbb{Z}^2)$, and (modulo translation in $\mathbb{T}^2$) each of these components is covered by an affine subspace of $C^1(\Gamma, \mathbb{R}^2)$.

Proposition 3.6.2. *Let $\rho \in H^1(\Gamma, \mathbb{Z}^2) \cong Im(d^0_{\mathbb{Z}})^\perp$. There is a surjective map*

$$\mathbb{T}^2 \oplus \left(\left(\rho + Im(d^0_{\mathbb{R}}) \right) \cap \widetilde{S} \right) \to \mathcal{M}_\rho(\Gamma)$$

that restricts to a covering map

$$\left(\mathbb{T}^2 \oplus \left(\left(\rho + Im(d^0_{\mathbb{R}}) \right) \cap \widetilde{S} \right) \right) \setminus \widetilde{D} \to \mathcal{M}_\rho(\Gamma)$$

where $\widetilde{D}$ denotes the preimage in $C^*(\Gamma, \mathbb{R}^2)$ of the degeneracy locus $D \subset C^*(\Gamma, \mathbb{T}^2)$.

To summarize, we can efficiently compute $\mathcal{M}(\Gamma)/\mathbb{T}^2$ as follows:

1. The maps $d^0_{\mathbb{Z}}, d^0_{\mathbb{R}}$ are essentially the adjacency matrix for the abstract graph Γ.
2. Choose an element
$$\rho \in \mathrm{Coker}(d^0_{\mathbb{Z}}) \cong \mathrm{Im}(d^0_{\mathbb{Z}})^\perp$$
and view it as an element of $C^1(\Gamma, \mathbb{R}^2)$.
3. The slope restrictions $\widetilde{S}$ are determined by the Tait-coloring of Γ and the assignment of slopes in $\mathbb{R}^2$ to edge colors.

4. We then have
$$\mathcal{M}_\rho(\Gamma)/\mathbb{T}^2 = (\rho + \mathrm{Im}(d^*_{\mathbb{R}})) \cap \widetilde{S}$$

5. Letting ρ vary in $H^1(\Gamma, \mathbb{Z}^2) \cong \mathrm{Im}(d^*_{\mathbb{Z}})^\perp$ yields the entire space $\mathcal{M}(\Gamma)/\mathbb{T}^2$.

In general, this method may overcount triple grid diagrams but this indeterminacy is exactly determined by the discrete subset $\widetilde{S} \cap C^1(\Gamma, \mathbb{Z}^2)$.

Chapter 4

Pants distances of knotted surfaces in 4-manifolds

4.1 The Invariants: $\mathcal{L}_3^{\mathcal{P}}$ and $\mathcal{L}_3^*$

A *pair of pants* is a planar surface with Euler characteristic equal to -1. We can equivalently think of it as a thrice-punctured sphere, a disk with two punctures or a once-punctured annulus. A *pants decomposition* of $\Sigma_{g,2b}$, a surface with boundary, is a collection of simple closed curves that split the surface into pairs of pants. For a closed surface, i.e when $b = 0$, the pants decomposition has $2g - 2$ pairs of pants and therefore $3g - 3$ curves. In general, there are $3g + 2b - 3$ curves in any pants decomposition. Σ is called an *admissible* surface if $3g + 2b - 3 > 0$.

The *dual curve graph* $\mathcal{C}^*(\Sigma)$ of a surface Σ is a simplicial complex where each vertex is a pants decomposition of the surface. Two vertices a, b are connected by an edge if their representatives differ by a single curve. Let $d^*(a, b)$ denote the number of edges in the shortest path in $\mathcal{C}^*(\Sigma)$ connecting a and b. Given two subsets $A, B \subset \mathcal{C}^*(\Sigma)$, the *distance* $d^*(A, B) = \min\{d^*(a, b) \mid a \in A, b \in B\}$ i.e. the minimum distance between A and B.

The *pants graph* $\mathcal{P}(\Sigma)$ is a subgraph of $\mathcal{C}^*(\Sigma)$. Two pants decompositions are connected by an edge if their representatives differ one of two moves: *A-move* or *S-move*. An A-move replaces a curve with another curve that intersects it geometrically twice but algebraically zero, and an S-move replaces a curve with another curve that intersects it once. See Figure 4.1. As before, let $d^{\mathcal{P}}(a, b)$ denote the graph length of a geodesic in $\mathcal{P}(\Sigma)$ connecting two vertices a and b, and for two subsets $A, B \subset \mathcal{P}(\Sigma)$, let $d^{\mathcal{P}}(A, B) = \min\{d^{\mathcal{P}}(a, b) \mid a \in A, b \in B\}$.

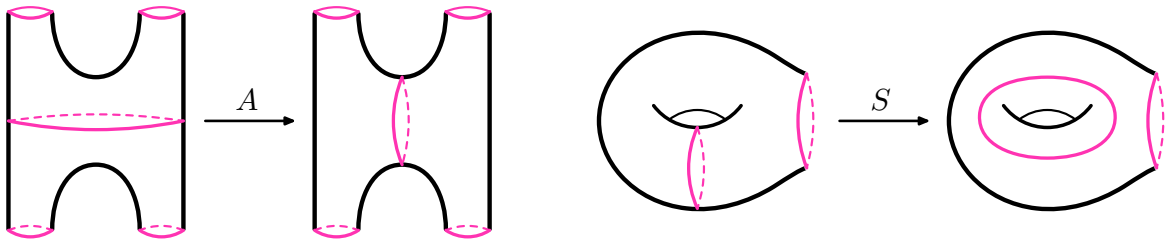

Figure 4.1: Local model of an A-move and S-move.

Now consider a three-dimensional handlebody H with a trivial tangle T in the context of Heegaard splittings and bridge decompositions. The boundary of H is a $2b$-punctured surface Σ of genus g. A curve in a surface Σ is *essential* if it does not bound a disk or once-punctured disk in Σ. A *c-disk* is an embedded disk in H whose boundary is an essential simple closed curve on Σ and whose interior intersects T at most once. If a c-disk does not intersect the tangle, it is called a *compressing disk*, and if it intersects the tangle once it is called a *cut disk*. The boundary of a compressing, resp. cut, disk is a compressing curve, resp. cut curve.

Restricting subcomplexes spanned by curves that bound disks in trivial tangles, a vertex v in the dual curve graph or the pants graph is said to belong to the *disk set* $\mathcal{D}(H,T)$ if each curve in the pants decomposition bounds a c-disk for (H,T).

Let $\mathcal{T}$ be a bridge multisection for a pair (X,F). The disk sets of the tangles (H_i,T_i), denoted by $\mathcal{D}_i$, are subsets of $\mathcal{P}(\Sigma)$ and therefore also of $\mathcal{C}^*(\Sigma)$. The distance between the disk sets of consecutive tangles is the same if computed in $\mathcal{C}^*(\Sigma)$ or $\mathcal{P}(\Sigma)$; that is, $d^*(\mathcal{D}_i,\mathcal{D}_{i+1}) = d^{\mathcal{P}}(\mathcal{D}_i,\mathcal{D}_{i+1})$, $\forall i = 1,\dots,n$. A pair of vertices $(u,v) \in \mathcal{D}_i \times \mathcal{D}_{i+1}$ is called an *efficient defining pair* for $(\mathcal{D}_i,\mathcal{D}_{i+1})$ if it achieves the (minimum) distance between $\mathcal{D}_i$ and $\mathcal{D}_{i+1}$.

The $\mathcal{L}$- and $\mathcal{L}^*$-invariants are capturing the complexity of the manifold by summing the distances between vertices which belong to efficient pairs for the disk sets. See Figure 4.2.

The $\mathcal{L}_n^*$*-invariant* of an n-section $\mathcal{T}$ is equal to smallest sum $\sum_i d^*(P_i', P_{i+1})$ amongst all efficient pairs (P_i,P_i') for $(\mathcal{D}_i,\mathcal{D}_{i+1})$. Analogously, the $\mathcal{L}_n^{\mathcal{P}}$*-invariant* of an n-section $\mathcal{T}$ is defined to be the minimum of $\sum_i d^{\mathcal{P}}(P_i', P_{i+1})$ amongst all efficient defining pairs (P_i,P_i') for $(\mathcal{D}_i,\mathcal{D}_{i+1})$.

Let F be a surface embedded in a closed 4-manifold X. The $\mathcal{L}_n^*$*-invariant* of the pair (X,F) is the smallest $\mathcal{L}_n^*(\mathcal{T})$ amongst all n-sections for (X,F) having minimal complexity (g,b). The $\mathcal{L}_n^{\mathcal{P}}$*-invariant* of (X,F) is defined the same way.

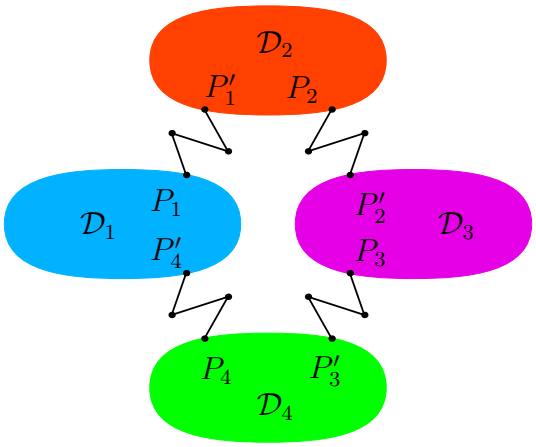

Figure 4.2: $\mathcal{L}_n^{\mathcal{P}}(\mathcal{T})$ and $\mathcal{L}_n^*(\mathcal{T})$ count the total number of edges between vertices for each disk set.

As that $\mathcal{P}(\Sigma)$ is a subgraph of $\mathcal{C}^*(\Sigma)$ with the same vertex set, $\mathcal{L}_n^* \leq \mathcal{L}_n^{\mathcal{P}}$. Therefore, a path in $\mathcal{P}(\Sigma)$ gives rise to a path in $\mathcal{C}^*(\Sigma)$, but not necessarily a geodesic. Because of this, many of results are stated (solely) in terms of the $\mathcal{L}_n^*$ version.

4.1.1 $\mathcal{L}$ and $\mathcal{L}^*$ are different invariants

The $\mathcal{L}$- and $\mathcal{L}^*$-invariants both count the number of edges between vertices in the disk sets, but the edges counted in the Kirby-Thompson invariant always lie in the disk sets, while the edges counted in our definition may go out of the disk sets, like the original Hempel distance of Heegaard splittings [Hem01].

It is natural to ask whether $\mathcal{L}$ and $\mathcal{L}^*$ are related. The following two results show that the two versions behave differently.

Theorem 4.1.1. *[Ara+23] There is an infinite family of 4-manifolds $\{X_p\}_{p\in\mathbb{N}}$ such that*

$$\sup_p \mathcal{L}_3^*(X_p) < \infty, \quad \sup_p \mathcal{L}(X_p) = \infty.$$

Theorem 4.1.2. *[Ara+23] There is an infinite family of 4-manifolds $\{Y_m\}_{m\in\mathbb{N}}$ such that*

$$\sup_m \mathcal{L}_3^*(Y_m) = \infty, \quad \sup_m \mathcal{L}(Y_m) = 0.$$

4.2 Examples

To calculate $\mathcal{L}$- invariant, we need to calculate the smallest sum of distances in the dual curve graph. As it is tedious to explore all possibilities, it is useful to utilize results which give us lower bounds for this purpose. For upper bounds, we can try to do methodical constructions.

For c-irreducible $(g, k; b, c)$-bridge trisections, the following theorem gives us a lower bound, which is helpful in calculating the $\mathcal{L}$- invariant for complex curves of degree 1 and 2 in $\mathbb{CP}^2$ (Example 4.2.2).

Theorem 4.2.1. *[Ara+23] Let $\mathcal{T}$ be a c-irreducible $(g, k; b, c)$-bridge trisection. Then,*

$$\mathcal{L}_3^*(\mathcal{T}) \geq 6g + 3b + (k_1 + k_2 + k_3) + (c_1 + c_2 + c_3) - 9.$$

Example 4.2.2. [Trisection of $\mathcal{C}_1$ and $\mathcal{C}_2$ in $\mathbb{CP}^2$] Let $\mathcal{C}_d$ denote the degree d complex curve in the complex projective plane. For $d = 1, 2$, $\mathcal{C}_d$ admits c-irreducible bridge trisections with complexities $(g, k; b, c) = (1, 0; 1, 1)$. The lower bound in Theorem 4.2.1 gives that $\mathcal{L}_3^* \geq 3$. For the upper bound, consult Figure 4.3. Note that each gray curve that moves once in each disk set is a reducing curve (bounds c-disks in two trivial tangles). Therefore, $\mathcal{L}_3^*(\mathbb{CP}^2, \mathcal{C}_1) = \mathcal{L}_3^*(\mathbb{CP}^2, \mathcal{C}_2) = 3$.

The following lemma is used in calculating the lower bound for Trisection of $\mathcal{C}_{1,1}$ in $S^2 \widetilde{\times} S^2$ (Example 4.2.4)

Lemma 4.2.3. *[Ara+23] Let (H, T), (H', T') be two (g, b)-trivial tangles whose union is a c-component unlink U_c in $Y_k := \#^k S^1 \times S^2$ in (g, b)-bridge position, with $\partial H = \partial H' = \Sigma$. Let (P, P') be an efficient pair for (H, T), (H', T'). Then the distance in $C^*(\Sigma)$ between P and P' is $d(P, P') = g - k + b - c$. Moreover, there is a geodesic λ connecting P to P' satisfying the following properties:*

1. *The path λ consists of $(g - k)$ S-moves and $(b - c)$ A-moves.*
2. *Every curve in P moves at most once, and furthermore:*
   (a) *every curve in P intersects at most one curve in P', and*
   (b) *if a curve in P intersects a curve in P', then they intersect in either one or two points.*
3. *Only compressing curves move.*

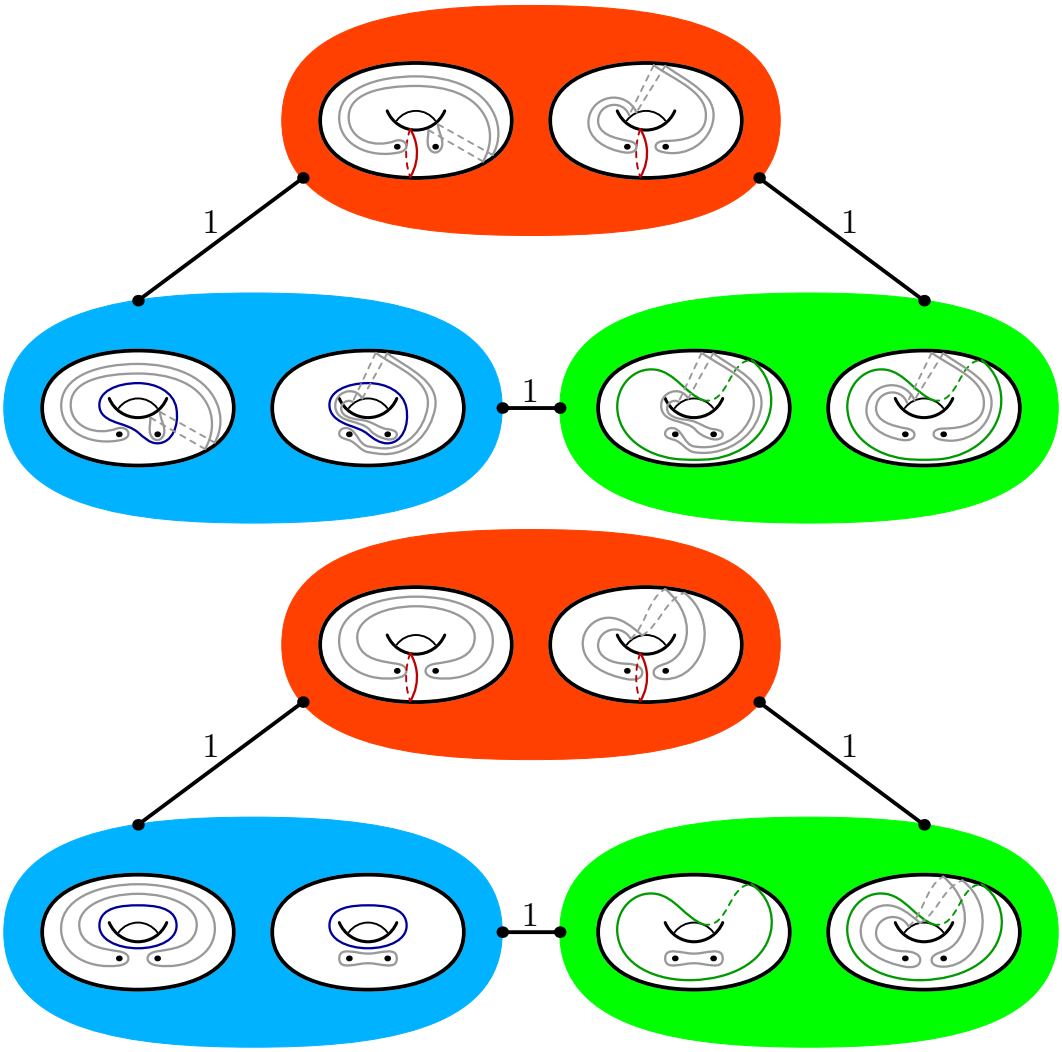

Figure 4.3: Loops in $\mathcal{C}^*(\Sigma_{1,2})$ estimating $\mathcal{L}_3^*$ for $(\mathbb{CP}^2, \mathcal{C}_1)$ (above) and $(\mathbb{CP}^2, \mathcal{C}_2)$ (below).

Example 4.2.4. [Trisection of $\mathcal{C}_{1,1}$ in $S^2\widetilde{\times}S^2$]

Consider the sphere $\mathcal{C}_{1,1}$ representing the homology class $(1,1)$ in $H_2(S^2\widetilde{\times}S^2,\mathbb{Z})$. Such a surface admits a bridge trisection diagram depicted in Figure 4.4 with complexity $(g,k;b,c) = (2,0;1,1)$. The number of curves in a pants decomposition is $3g+2b-3 = 5$. The curves that are not colored grey are the ones that move outside the disk sets and are not contributing to the count of $\mathcal{L}_3^*$. Among these grey curves, there is one curve λ that stays fixed along the whole loop. Each of the remaining grey curves moves once. Since there are three disk sets, we get the upper bound $\mathcal{L}_3^*(S^2\widetilde{\times}S^2,\mathcal{C}_{1,1}) \leq 6$.

To estimate the lower bound, let us focus on the depicted edge connecting red and blue handlebodies. Lemma 4.2.3 tells us that there are two separating curves, each cutting off a genus one summand bounding in red and blue handlebodies simultaneously. If these two curves stay stationary in the red disk set, then we get two grey curves λ_1 and λ_2 that bound in three disk sets simultaneously. This implies that the surface $\mathcal{C}_{1,1}$ is completely contained in a $\mathbb{CP}^2$ summand or a $\overline{\mathbb{CP}^2}$ summand. This cannot happen since $\mathcal{C}_{1,1}$ generates homology in both summands. Thus, λ_1 and λ_2 each moves at least once. Making the same argument for the red-green pair and the blue-green pair gives $\mathcal{L}_3^*(\mathcal{C}_{1,1}) = 6$.

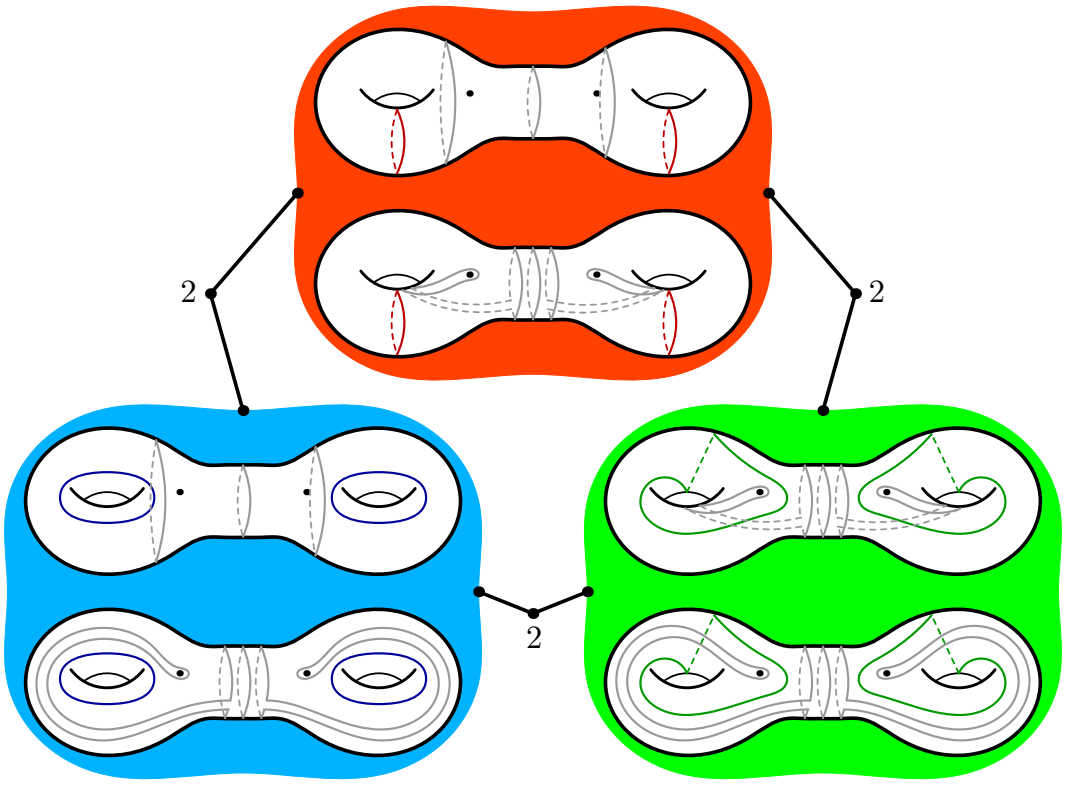

Figure 4.4: A loop in the dual curve graph giving $\mathcal{L}_3^*(S^2\widetilde{\times}S^2,\mathcal{C}_{1,1}) \leq 6$.

A multisection $\mathcal{T}$ is *completely decomposable* if it can be c-reduced into a collection of multisections of complexities $(g,b) \in \{(0,1),(0,2),(1,0)\}$. In other words, completely decomposable multisections are c-connected sums and self-tubings of bridge multisections with the lowest complexities.

Theorem 4.2.5. *[Ara+23] Let $\mathcal{T}$ be a multisection with $\mathcal{L}^*(\mathcal{T}) \leq 1$. Then $\mathcal{T}$ is completely decomposable.*

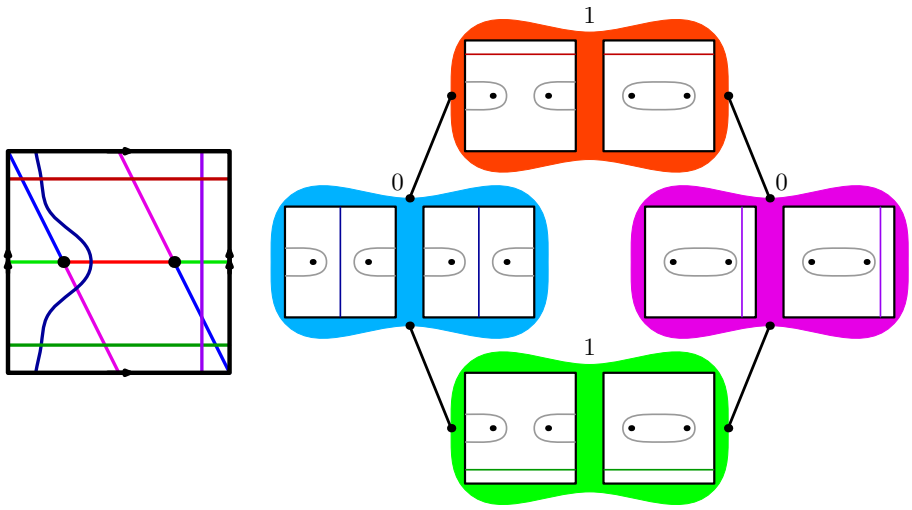

Figure 4.5: A diagram for $(S^2 \times S^2, S^2 \times \{pt\})$ and a loop showing that $\mathcal{L}^* \leq 2$.

Example 4.2.6. [Quadrisection of $S^2 \times \{\text{pt}\} \subset S^2 \times S^2$] Consider the surface $F = S^2 \times \{\text{pt}\} \subset S^2 \times S^2$. By work of [Isl+22], this admits a multisection with $(g,b) = (1,1)$ depicted in Figure 4.5. Since this quadrisection is c-irreducible, i.e not completely decomposable, Theorem 4.2.5 implies that $\mathcal{L}^*_4 \geq 2$. On the other hand, the loop in Figure 4.5 shows that $\mathcal{L}^*_4 \leq 2$ and so $\mathcal{L}^*_4(S^2 \times S^2, S^2 \times \{\text{pt}\}) = 2$.

4.3 Results

Detection results

A good feature of Kirby-Thompson's $\mathcal{L}$-invariant is that it detects the 4-sphere: if X is a homology 4-sphere with $\mathcal{L}(X) \leq 1$, then X is diffeomorphic to the 4-sphere. Similar results hold for the $\mathcal{L}$-invariants of 4-manifolds with boundary [Cas+22] and surfaces in S^4 [Bla+20]. We present an incarnation of the now classic detection result for $\mathcal{L}^*_n$-invariants of (4-manifold, surface) pairs.

Theorem 4.3.1. *Let F be an embedded surface in a closed 4-manifold X with no $S^1 \times S^3$ summands. If $\mathcal{L}_n^*(X,F) \leq 1$ for some $n \geq 3$, then F is smoothly isotopic to an unknotted surface in $X = \#^i S^2 \times S^2 \#^j \mathbb{CP}^2 \#^k \overline{\mathbb{CP}^2}$.*

This bound is the best possible as Example 4.2.6 exhibits a complex curve in $\mathbb{CP}^1 \times \mathbb{CP}^1$ of bi-degree (1,0) with $\mathcal{L}_4^* = 2$. We have proved stronger results: we classify multisections with complexity at most two in [Ara+23]. Recently, Ogawa improved the detection result for Kirby-Thompson's $\mathcal{L}$-invariant, showing that in fact, $\mathcal{L}(X) \leq 2$ implies that X is diffeomorphic to the 4-sphere [Oga21]. We prove that the same result holds for $\mathcal{L}_3^*$. The following is a stronger version of [APZ22, Theorem 3.5].

Theorem 4.3.2. *[Ara+23] Let F be an embedded surface in a closed 4-manifold X with no $S^1 \times S^3$ summands. If $\mathcal{L}_3^*(X,F) \leq 2$, then F is smoothly isotopic to an unknotted surface in $X = \#^i S^2 \times S^2 \#^j \mathbb{CP}^2 \#^k \overline{\mathbb{CP}^2}$.*

As with other meaningful invariants, it is natural to ask whether our complexity can be arbitrarily large. We give a positive answer to this question in the following theorem, and remark that when X is diffeomorphic to S^4, we recover [APZ22, Theorem 1.1].

A 4-manifold is *prime* if in every connected sum decomposition, one summand is S^4. In the same spirit, a knotted surface is *prime* if it is nontrivial and if in every connected sum decomposition, one summand is is a trivial 2-knot. A pair (X,F) is prime if both X and F are prime.

Theorem 4.3.3. *[Ara+23] Let (X,F) be a prime (4-manifold, surface) pair. Then,*

$$\mathcal{L}_3^*(X,F) \geq 7(g-1) - \chi(X) + 4b + \chi(F),$$

where (g,b) are the smallest trisection genus and bridge number of the pair (X,F).

Classification of genus two quadrisections

Genus two trisections were shown to be standard by Meier and Zupan [MZ17b], but the classification of genus three trisections is still open. A complete list of manifolds admitting genus three trisections was proposed by Meier [Mei18]. Progress towards this problem was made by Armand and Moeller [AM22], where various trisection diagrams were shown to belong to Meier's list.

An advantage of multisections is that generally speaking, a 4-manifold may be represented by a central surface of a lower genus [IN20, Theorem 8.4]. In their work, Naylor and Islam-

bouli showed that 4-manifolds admitting genus two quadrisections form a subfamily of all 4-manifolds admitting genus three trisections. This leads to the following problem.

Problem 4.3.4. *Classify 4-manifolds admitting genus two quadrisections.*

We solve the problem for 4-manifolds with $\mathcal{L}_4^*$-invariant at most six.

Theorem 4.3.5. *[Ara+23] Let X be a 4-manifold with a $(2,1)$-quadrisection $\mathcal{T}$. If $\mathcal{L}_4^*(\mathcal{T}) \leq 6$, then X is diffeomorphic to the spin of a lens space, the twisted-spin of a lens space, $\#^2 S^1 \times S^3$, or $\#^h S^1 \times S^3 \#^i S^2 \times S^2 \#^j \mathbb{CP}^2 \#^k \overline{\mathbb{CP}^2}$ where $h = \{0, 1\}$.*

Bridge distance in dimension three

The three-dimensional version of $\mathcal{L}^*$ is an invariant $D(\Sigma)$ introduced by Zupan in [Zup13]. $D(\Sigma)$ measures the distance between the disk sets in the bridge splitting of a link in a closed 3-manifold. He showed that if K is a knot and M has no $S^1 \times S^2$ summands, then (g, b)-bridge positions of (M, K) have complexity $D(\Sigma)$ at least $g + b - 1$. In particular, the distance zero splittings are 1-bridge unknots in S^3. The main technical lemma is a result in the same vein as Zupan's.

Lemma 4.3.6. *[Ara+23] Let Σ be a (g, b)-bridge splitting of an unlink in $\#^k S^1 \times S^2$. Then $D(\Sigma)$ is exactly $g - k + b - c$.*

We conjecture that these results can be merged together as follows.

Conjecture 4.3.7. Let K be a c-component link embedded in a compact 3-manifold M with k $S^1 \times S^2$ summands. For any (g, b)-bridge position of (M, K),

$$D(\Sigma) \geq g - k + b - c.$$

Moreover, equality holds if and only if K is an unlink in $\#^k S^1 \times S^2$.

Chapter 5

Quasiquadruple grid diagrams for surfaces in $\mathbb{CP}^1 \times \mathbb{CP}^1$

5.1 Motivation

A grid diagram is a collection of points on a toroidal grid which realises a link in $\mathbb{S}^3$. They can be interpreted as a front projection of a Legendian link in the standard contact $\mathbb{S}^3$. This notion was generalised to that of a triple grid diagram, which simultaneously encodes three such Legendrian links and (under certain circumstances) a Lagrangian surface in $\mathbb{CP}^2$ [BGL23]. The work in this chapter, which is joint with Fushida-Hardy and Wakelin, defines a similar notion for $\mathbb{CP}^1 \times \mathbb{CP}^1$.

Notice that exactly like $\mathbb{CP}^2$,$\mathbb{CP}^1 \times \mathbb{CP}^1$ admits a genus-1 multisection diagram (Figure 5.1) such that taking pairs of consecutive multisection curves on $\mathbb{T}^2$ generates a Heegaard diagram for $\mathbb{S}^3$. Additionally, $\mathbb{CP}^1 \times \mathbb{CP}^1$ can be equipped with the usual Fubini-Study symplectic form on each factor, making it a sympletic manifold ($\mathbb{CP}^1 \times \mathbb{CP}^1$,$\omega$).

We can see that $(X, \omega, \mathbb{T}^2, \mu)$ is a symplectic toric manifold. Consider projective coordinates on $X = \mathbb{CP}^1 \times \mathbb{CP}^1$, given by

$$\mathbb{CP}^1 \times \mathbb{CP}^1 = \{(x, y) = ([x_0 : x_1], [y_0 : y_1]) \mid x_0, x_1, y_0, y_1 \in \mathbb{C}\}.$$

The symplectic form is given by

$$\omega = -\frac{i}{2}\partial\overline{\partial}\log(|x_0|^2 + |x_1|^2) - \frac{i}{2}\partial\overline{\partial}\log(|y_0|^2 + |y_1|^2).$$

Writing $\mathbb{T}^2 = \{(\theta, \phi) \mid \theta, \phi \in [0, 2\pi)\}$, we have a toric action on X given by

$$(\theta, \phi) \cdot ([x_0 : x_1], [y_0 : y_1]) = ([x_0 : e^{i\theta} x_1], [y_0 : e^{i\phi} y_1]).$$

Take the product moment map $\mu : X \to \mathbb{R}$ given by

$$\mu(x, y) = \Big(\frac{|x_0|^2}{|x_0|^2 + |x_1|^2}, \frac{|y_0|^2}{|y_0|^2 + |y_1|^2} \Big).$$

The moment map associated to this symplectic toric manifold gives rise to a canonical 4-section, where the central quadsection surface is a torus, in a manner identical to $\mathbb{CP}^2$. Therefore, a natural next step is to define a notion analogous to triple grid diagram for $\mathbb{CP}^1 \times \mathbb{CP}^1 \cong \mathbb{S}^2 \times \mathbb{S}^2$.

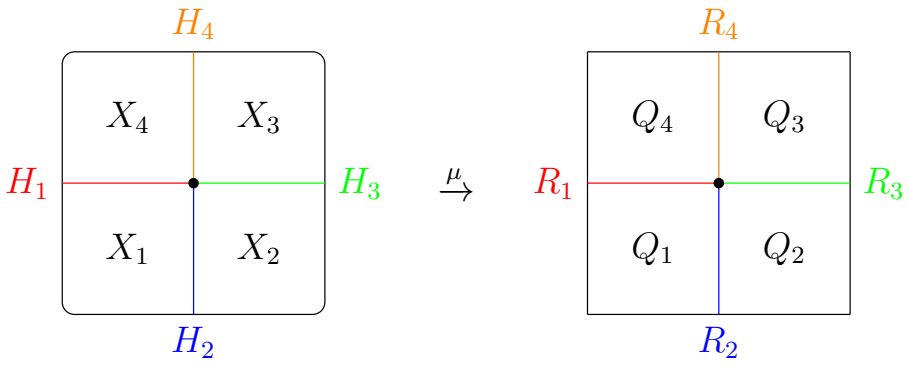

Figure 5.1: Genus 1 4-section of $\mathbb{CP}^1 \times \mathbb{CP}^1$

Definition 5.1.1. A *quadruple grid diagram* of grid number n is an $n \times n$ grid diagram with $2n$ dots encoding the four links in each sector of $\mathbb{CP}^1 \times \mathbb{CP}^1$. It can be broken down into Red-Blue, Blue-Green, Green-Orange, and Orange-Red grid diagrams.

Definition 5.1.2. A *Red-Blue* Legenrian grid diagram is the grid diagram corresponding to the sector of $\mathbb{CP}^1 \times \mathbb{CP}^1$ which has boundary $H_1 \cup H_2$ i.e. corresponds to the red and blue sections of the multisection. The arcs obtained by joining the two dots in each row/column correspond to the shadow arcs in the corresponding handle body. Therefore, the *Red-Blue* grid diagram gives us a grid diagram of a Legendrian link in $H_1 \cup H_2$. In the same way, we can define *Blue-Green*, *Green-Orange*, and *Orange-Red* grid diagrams.

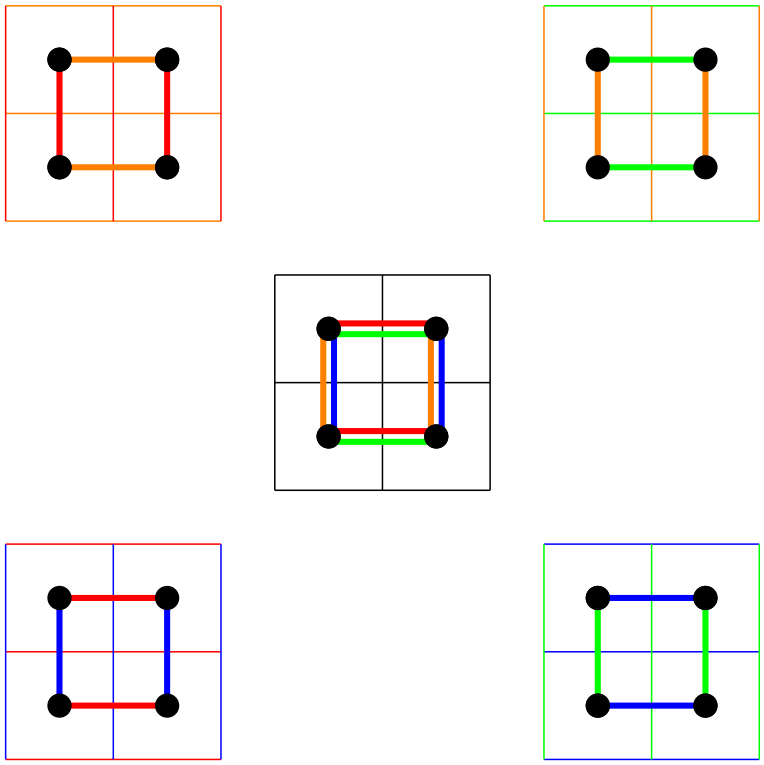

Figure 5.2: A quadruple grid diagram (centre) representing the torus in $\mathbb{CP}^1 \times \mathbb{CP}^1$ via the four associated Legendrian grids.

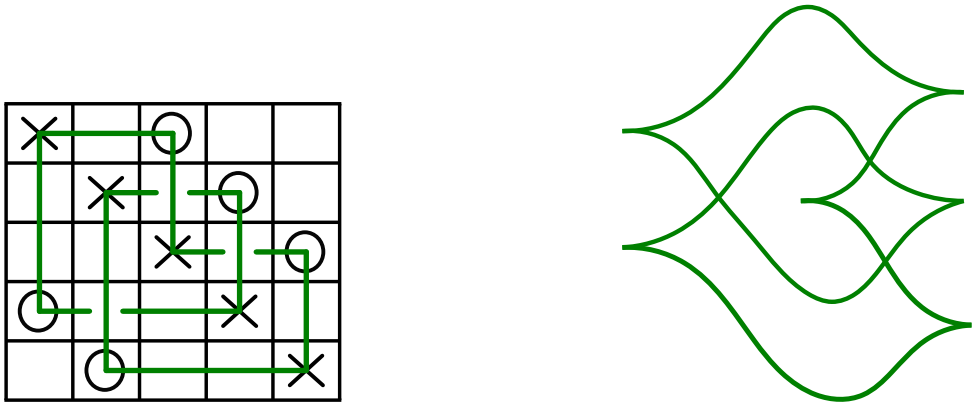

Figure 5.3: Example of grid diagram to Legendrian projection

Once we have a grid diagram for the Legendrain link in $H_1 \cup H_2$, we can obtain the Legendrian projection by rotating the grid $\pi/4$ in the clockwise direction and smoothing the local maxima and minima as shown in Figure 5.3.

In the case of $\mathbb{CP}^1 \times \mathbb{CP}^1$, the inherent symmetry of the standard genus one multisection would force any associated *quadruple grid diagram* to obey a strict series of combinatorial restrictions, severely limiting their utility: it turns out that the only quadruple grid diagram which can actually exist is the one which encodes the Lagrangian torus in $\mathbb{CP}^1 \times \mathbb{CP}^1$. This is corroborated by the previously established fact that the only Lagrangian immersion of (orientable compact) surfaces in $\mathbb{CP}^1 \times \mathbb{CP}^1$ are spheres and tori [CU06].

Lemma 5.1.3. *There is only one possible Lagrangian quadruple grid diagram in* $\mathbb{CP}^1 \times \mathbb{CP}^1$.

Proof. Let there be a quadruple grid diagram of size n which has $2n$ points. By definition, this encodes the Legendrian diagram in $\mathbb{S}^3$ obtained in each sector X_i of the multisection diagram of $\mathbb{CP}^1 \times \mathbb{CP}^1$ when looking at the colors pairwise in order — Red-Blue, Blue-Green, Green-Orange, and Orange-Red.

Due to the symmetry of the multisection of $\mathbb{CP}^1 \times \mathbb{CP}^1$, the Red-Blue and Green-Orange projections obtained from the quadruple grid diagram are always the same. Similarly, the Blue-Green and Orange-Red projections are always the same. Hence we get this Table 5.1 of cusps and writhe.

	Red Blue	Blue Green	Green Orange	Orange Red
cusps	c_1	c_2	c_1	c_2
writhe	w_1	w_2	w_1	w_2

Table 5.1: Cusps and Writhe of a Quadruplre Grid Diagram

Let the Red-Blue and Green-Orange projections be Diagram 1 and the Blue-Green and-Orange Red projections be Diagram 2. Note that every point in the grid diagram is a cusp in either Diagram 1 or Diagram 2, i.e. $4n = 2c_1 + 2c_2$. Furthermore, the sign of a crossing in Diagram 1 is the opposite of its sign in Diagram 2. So $w_1 = -w_2$.

Recall that the we are looking at Legendrian diagrams i.e. $tb = -1$ and $rot = 0$ for all four projections, giving us the following equations.

$$w_1 - \frac{1}{2}c_1 = -1$$

$$w_2 - \frac{1}{2}c_2 = -1$$

Combining the above facts, we get $n = 2$ as the only non-trivial solution. So the only Lagrangian quadruple grid giagram in $\mathbb{CP}^1 \times \mathbb{CP}^1$ is Figure 5.2 which represents $\mathbb{T}^2$. □

5.2 Quasiquadruple grid diagrams

As the quadruple grid diagram definition is very restrictive Lemma 5.1.3, a different approach with more flexibility was the next step. For this, we utilize a specific decomposition of $\mathbb{S}^2 \times \mathbb{S}^2$ which does not quite fit the definition of a Weinstein multisection. Instead, we will introduce the notion of a *Weinstein decomposition*, which can be thought of as a symplectic version of a polyhedral decomposition (introduced in [Lam21]).

Definition 5.2.1. A *Weinstein decomposition* $\mathcal{W}$ of a symplectic 4-manifold (X, ω) is a Whitney stratification of X satisfying the following conditions.

1. the closure of each open stratum is a compact manifold with corners;
2. each 4-dimensional stratum $(X_i, \omega|_{X_i})$ admits the structure of a Weinstein domain: namely, there exists a Liouville vector field $\rho_i : X_i \to TX_i$ which is outwardly transverse to the boundary ∂X_i and a Morse function $f_i : X_i \to \mathbb{R}$ for which ρ_i is gradient-like.

Remark 5.2.2. Every symplectic manifold admits a compatible almost-complex structure. A Weinstein decomposition is a special case of a polyhedral decomposition as defined in [Lam21].

We thicken the central torus of the standard genus one Weinstein multisection of $\mathbb{CP}^1 \times \mathbb{CP}^1$ to $\mathbb{D}^1 \times \mathbb{T}^2$, thus producing a *Weinstein decomposition* of $\mathbb{CP}^1 \times \mathbb{CP}^1$: a stratification satisfying certain properties regarding convexity and symplectic structure. This has the effect of allowing some extra freedom in two of the four grids, leading to the definition of a quasiquaduple grid diagram.

Our choice of decomposition of X arises from the division of the moment polygon depicted in Figure 5.4. The *quasiquadrants* Q_1, Q_2, Q_3, Q_4 of the moment polygon lift to the *quasisectors* X_1, X_2, X_3, X_4 of X which intersect consecutively along solid tori H_1, H_2, H_3, H_4. This almost gives a multisection, but, instead of a single central surface $\Sigma \cong \mathbb{T}^2$, we have two disjoint tori, $\Sigma^- = \mathbb{T}^2_{\frac{1}{\sqrt{3}}}$ and $\Sigma^+ = \mathbb{T}^2_{\sqrt{3}}$, which cobound a supplementary handlebody $H_0 = \mathbb{T}^2 \times [\frac{1}{\sqrt{3}}, \sqrt{3}]$.

Definition 5.2.3. A *combinatorial quasiquadruple grid diagram* of grid number n and size b is an $n \times n$ grid, together with a collection of $2b$ (possibly trivial) oriented disjoint line

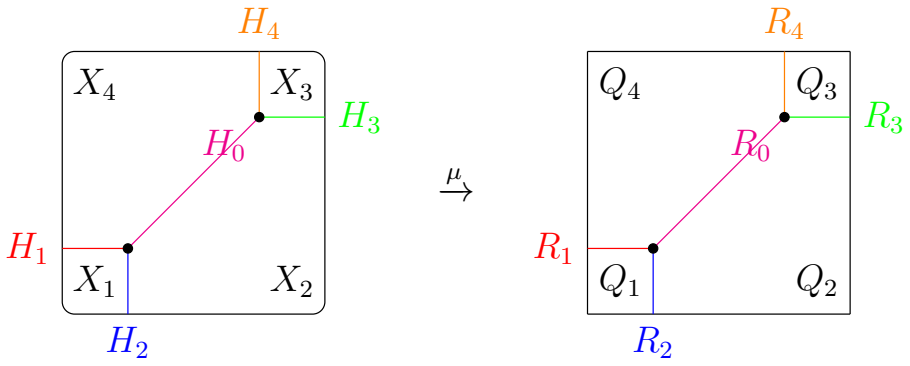

Figure 5.4: Genus 1 quasiquadsection of $\mathbb{CP}^1 \times \mathbb{CP}^1$.

segments, which connect a set of marked points Θ^- to another set of marked points Θ^+, such that:

- the total set of marked points $\Theta = \Theta^+ \cup \Theta^-$ lies in the centres of squares of the grid;
- each set of marked points Θ^- and Θ^+ forms a grid diagram;
- each of the line segments has gradient 1.

The grid is indexed modulo n: a line segment may exit the grid to the right and reappear from the left, and similarly for top and bottom. However, any such line segment must terminate before reaching its starting point.

A non-trivial example of a quasiquadruple grid diagram is shown in Figure 5.5, which represents the antidiagonal sphere, along with the associated Legendrian grids, demonstrating the advantage of the additional flexibility offered by quasiquadruple grid diagrams.

Definition 5.2.4. A quasiquadruple grid diagram has *Property L* if each of the induced Legendrian link diagrams RB, BPG, GO and OPR are unlinks with Thurston-Bennequin number -1.

Definition 5.2.5. A *geometric quasiquadruple grid diagram* is a thickened torus $\mathbb{T}^2 \times [\frac{1}{\sqrt{3}}, \sqrt{3}]$, together with a piecewise linear tangle $P \subset \mathbb{T}^2 \times [\frac{1}{\sqrt{3}}, \sqrt{3}]$, such that:

- each component of P has one endpoint in $\mathbb{T}^2 \times \{\frac{1}{\sqrt{3}}\}$ and the other in $\mathbb{T}^2 \times \{\sqrt{3}\}$;

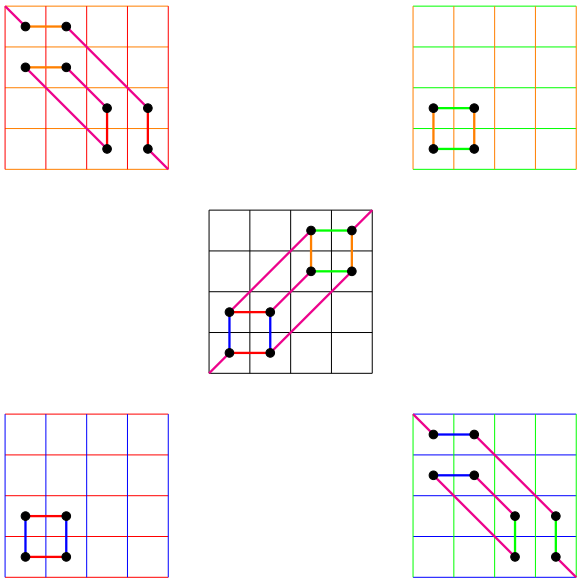

Figure 5.5: A quasiquadruple grid diagram (centre) representing the antidiagonal sphere in $\mathbb{CP}^1 \times \mathbb{CP}^1$ via the four associated Legendrian grids.

- the intersections $\Theta^- := P \cap (\mathbb{T}^2 \times \{\frac{1}{\sqrt{3}}\})$ and $\Theta^+ := P \cap (\mathbb{T}^2 \times \{\sqrt{3}\})$ are grid diagrams;
- outside the central torus $\mathbb{T}^2 \times \{1\}$, each component of P is parallel to the z-axis;
- inside the central torus $\mathbb{T}^2 \times \{1\}$, each component of P is parallel to the line $x = y$.

5.3 Moduli Space of Quasiquadruple Grid Diagrams

From [GL24], we have the insight that focusing on the underlying graph not only generates interesting examples, but also gives us the moduli space of all possibilities. To apply the same approach for quasiquadruple grid diagrams, we need to first define the abstract graphs which will generate quasiquadruple grid diagrams. In order to do this, we relax rigid grid restrictions and instead consider geometric quasiquadruple grid diagrams, which correspond to immersions of *compatible* abstract graphs into $\mathbb{T}^2$.

Definition 5.3.1. A graph Γ is said to be *compatible* if Γ is cubic and has an edge-coloring such that each vertex in Γ has edges either {red,blue,pink} or {green,orange,pink}.

One way to construct compatible abstract graphs is as follows. Let Γ_+ be an abstract graph of b vertices, made up of cycle graphs of even length. Then, the edges of Γ_+ can be

colored with two colors, red and blue. Let Γ_- be another such abstract graph of b vertices, colored with green and orange. Then we can connect each vertex of Γ_+ to a vertex of Γ_- with a pink edge to get a cubic graph Γ, with $2b$ vertices, such that the blue, pink and green edges, and also the orange, pink and red edges, give us sub-graphs made up of cycles respectively. This is necessary as the sub-graph corresponding to each section of the quasiquadsection is a link.

Example 5.3.2. Let Γ_+ and Γ_- be made of two cycles of four vertices each (as seen in red-blue and green-orange grids of Figure 5.7). Let Γ be made out of connecting Γ_+ and Γ_- such that each red-blue cycle is connected with pink edges to both of the green-orange cycles such that Γ is compatible. Then Γ respresents a torus $\mathbb{T}^2$, as seen in the quasiquadruple grid diagram in Figure 5.7. The red-pink-orange grid diagram represents the link L6a1 according to the Thistlethwaite Link Table.

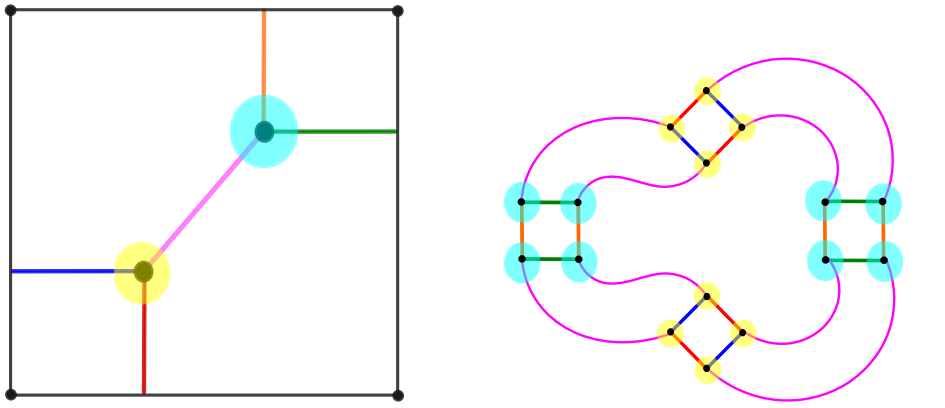

(a) $\mathbb{CP}^1 \times \mathbb{CP}^1$ moment polytope (b) Compatible graph representing $\mathbb{T}^2$

Figure 5.6: $\mathbb{CP}^1 \times \mathbb{CP}^1$ moment polytope with compatible graph

Theorem 5.3.3. *Let Γ be compatible graph with $2b$ vertices. The moduli space $\mathcal{M}(\Gamma)$ of geometric quasiquadruple grid diagrams with graph-type Γ is a smooth manifold of dimension greater than or equal to b.*

Proof. We can modify Lemma 3.4.4, which gives a lower bound for the dimension of the based moduli space of geometric triple grid diagrams corresponding to a cubic, Tait-colored abstract graph. Note that only S in the lemma, coming from the slope restrictions, is dependent on the coloring of the abstract graph.

In the case of quasiquadruple grid diagrams, the underlying graph is also trivalent, while having more colors. While this does modify the slope restrictions, the dimension of S remains

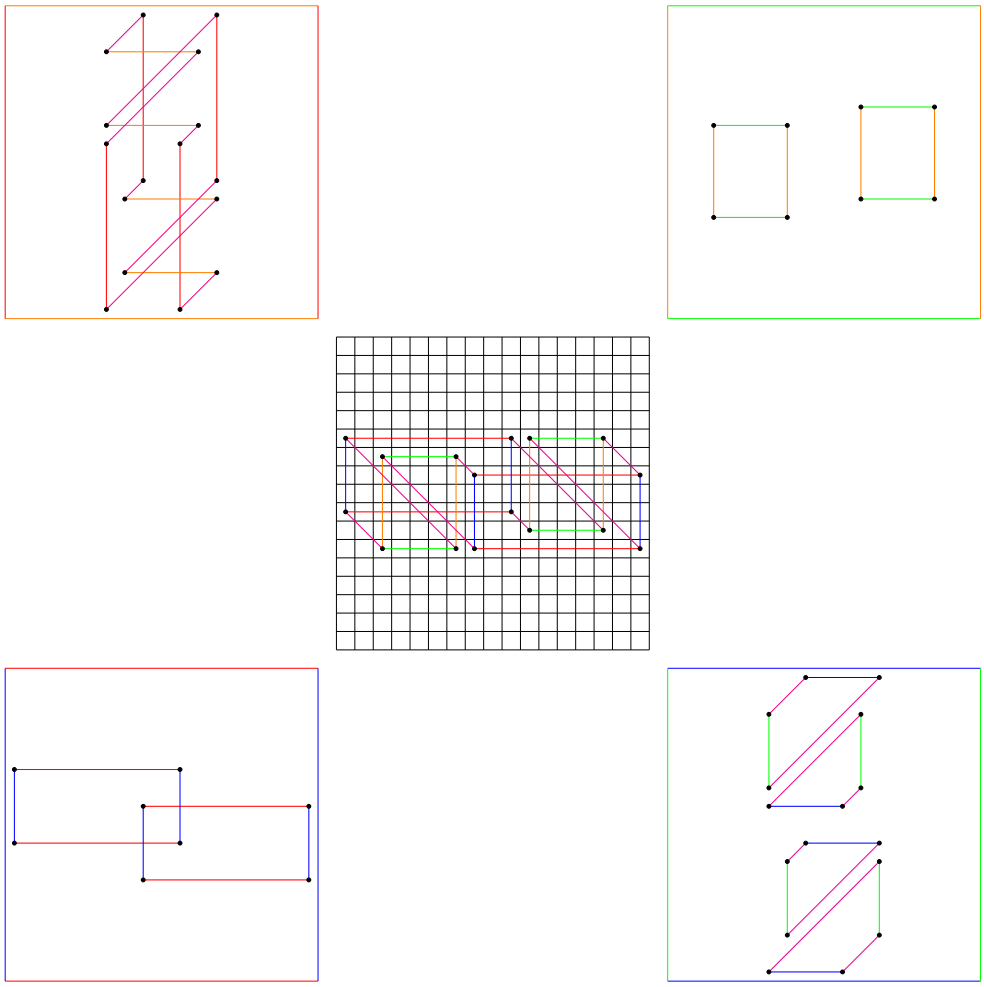

Figure 5.7: A quasiquadruple grid diagram representing $\mathbb{T}^2$

the same. This is because the dimension of S is still half the dimension of $C^1(\Gamma, \mathbb{T}^2)$, as each 1-cochain is constrained to lie in a 1-dimensional subspace of $\mathbb{T}^2$. Also, the dimension of $C^1(\Gamma, \mathbb{T}^2)$ is dependent only on the number of edges of Γ.

Therefore, $\dim \mathcal{M}_0(\Gamma) \geq b - 2$ i.e the based space of possible immersions of Γ into $\mathbb{T}^2$, is non empty if $b \geq 2$.

□

5.4 Future Directions

5.4.1 Lagrangian Surfaces in $\mathbb{CP}^1 \times \mathbb{CP}^1$

By adapting the approach followed in [BGL23], we can construct embedded Lagrangian surface in $\mathbb{CP}^1 \times \mathbb{CP}^1$ from quasiquadruple grid diagrams satisfying Property L. The outline of the proof is as follows.

We first explain how each of the four associated grid diagrams represents a Legendrian link in the standard contact $\mathbb{S}^3$. We do this by joining marked points with piecewise linear arcs which are everywhere tangent to the contact planes in the relevant contact 3-manifolds with boundary; we then explain precisely how to smooth the arcs in a way which is compatible with the contact structure to end up with a Legendrian link. By thickening up the union of our 3-dimensional strata, we show that these Legendrian links arise as the boundary of a Lagrangian cap in $(\mathbb{CP}^1 \times \mathbb{CP}^1) \setminus \cup_{i=1}^4 \mathbb{D}_i^4$. Finally, given that all four of these Legendrian links satisfy Property L, we are able to fill the boundary with Lagrangian slice discs in each $\mathbb{D}_i^4$ and end up with an closed Lagrangian surface embedded in $\mathbb{CP}^1 \times \mathbb{CP}^1$.

5.4.2 Extension to Toric Symplectic 4-manifolds

Triple grid diagrams have been defined for $\mathbb{CP}^2$ by Blackwell, Gay and Lambert-Cole. This was extended to $\mathbb{CP}^1 \times \mathbb{CP}^1$ by defining quasiquadruple grid diagrams which required slightly modifying the moment map for additional flexibility. This can be further extended to toric symplectic 4-manifolds as the moment polytope can be decomposed into polygonal bidisks by trivalent graphs [Lam21]. Additionally, we can define geometric n-tuple grid diagrams which correspond to immersions of certain abstract cubic graphs into $\mathbb{T}^2$ for toric symplectic 4-manifolds.

Geometric n-tuple grid diagrams

Definition 5.4.1. Consider a moment polytope having k exterior faces. Chose a proper embedding of a tree G with each k exterior vertices going to a unique exterior face of the polytope. Let each of $2k-3$ edges of graph G have a unique color associated to it. Then a graph Γ is said to be *compatible* with this decomposition if Γ is cubic and has an edge-coloring such that each vertex in Γ locally resemble one of the $(k-2)$ interior vertices of G.

Definition 5.4.2. A *geometric n-tuple grid diagram* is an immersion of a graph compatible with a moment polytope decomposition for a toric sympletic 4-manifold, having n exterior faces, into $\mathbb{T}^2$ such that edges of a color map to arcs with a corresponding rational slope.

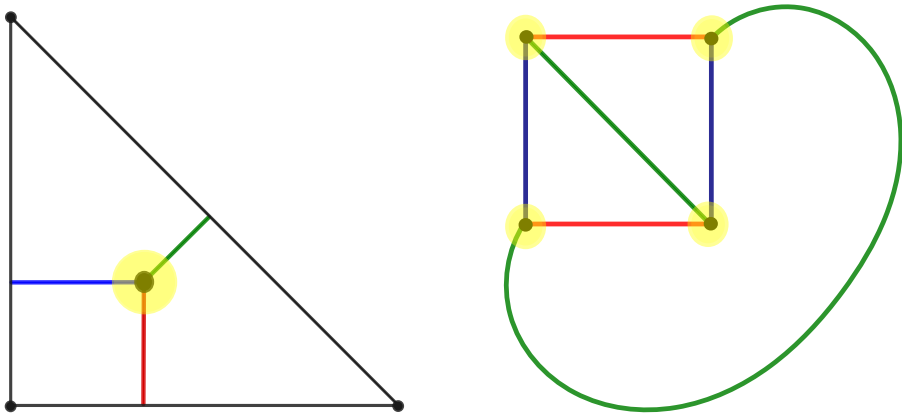

(a) $\mathbb{CP}^2$ moment polytope (b) Compatible graph representing $\mathbb{RP}^2$

Figure 5.8: $\mathbb{CP}^2$ moment polytope with a compatible graph

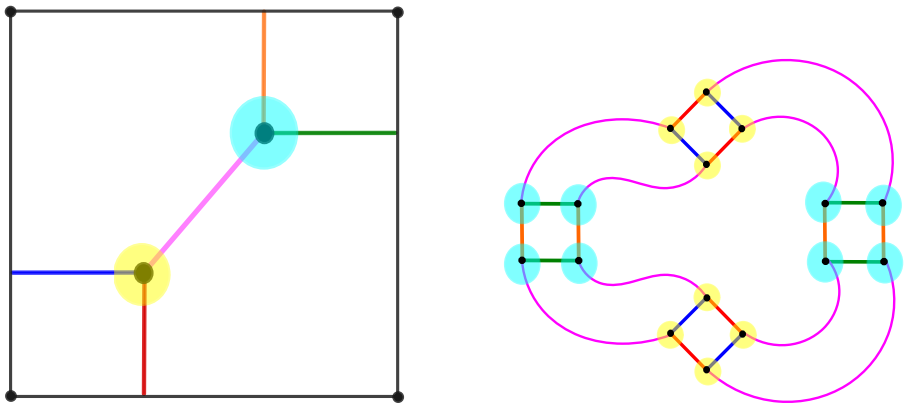

(a) $\mathbb{CP}^1 \times \mathbb{CP}^1$ moment polytope (b) Compatible graph representing $\mathbb{T}^2$

Figure 5.9: $\mathbb{CP}^1 \times \mathbb{CP}^1$ moment polytope with a compatible graph

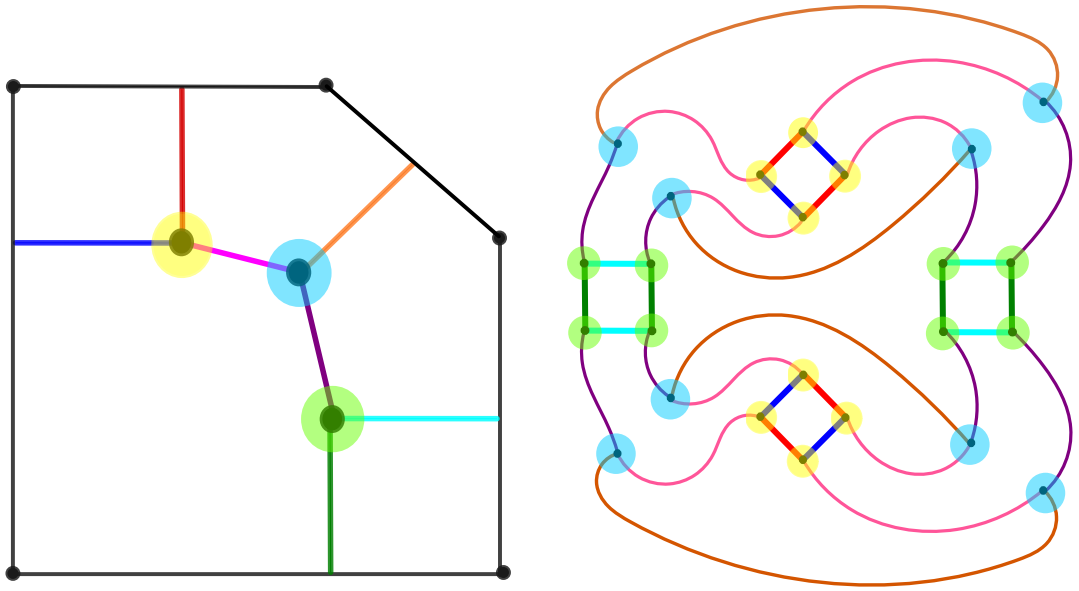

(a) $\mathbb{CP}^1 \times \mathbb{CP}^1 \# \overline{\mathbb{CP}}^2$ moment polytope (b) Compatible graph representing $\mathbb{T}^2 \# \mathbb{T}^2$

Figure 5.10: $\mathbb{CP}^1 \times \mathbb{CP}^1 \# \overline{\mathbb{CP}}^2$ moment polytope with a compatible graph

Theorem 5.4.3. *Let Γ be a compatible graph for a moment polytope decomposition of a toric symplectic manifold, with $2b$ vertices. The moduli space $\mathcal{M}(\Gamma)$ of geometric quasiquadruple grid diagrams with graph-type Γ is a smooth manifold of dimension greater than or equal to b.*

Proof. The proof of Theorem 5.3.3 illustrates that the dimension count of the moduli space is not dependent on the number of colors and slope restrictions. Hence, the result follows from Lemma 3.4.4 in exactly the same manner as for geometric quasiquadruple grid diagrams. □

Bibliography

[AM22] Román Aranda and Jesse Moeller. "Diagrams of $*$-trisections". In: *Mathematical Research Letters* 29.6 (2022), pp. 1595–1658 (↑ 36).

[APZ22] Román Aranda, Puttipong Pongtanapaisan, and Suixin Zhang. "Bounds for Kirby-Thompson invariants of knotted surfaces". In: *arXiv preprint arXiv:2206.02936* (2022) (↑ 3, 36).

[Ara+23] Román Aranda et al. *Pants distances of knotted surfaces in 4-manifolds*. 2023. arXiv: `2307.13874 [math.GT]` (↑ 31, 32, 35–37).

[Aud90] Michèle Audin. "Quelques remarques sur les surfaces lagrangiennes de Givental". In: *Journal of Geometry and Physics* 7.4 (1990), pp. 583–598 (↑ 13).

[Bla22] Sarah Blackwell. "Combinatorial and Group Theoretic Approaches to Trisected Surfaces in 4-Manifolds". eng. PhD thesis. University of Georgia, 2022, p. 108 (↑ 1).

[BGL23] Sarah Blackwell, David T. Gay, and Peter Lambert-Cole. *Constructing Lagrangians from triple grid diagrams*. 2023. arXiv: `2306.16404 [math.GT]` (↑ 1, 12, 14, 38, 47).

[Bla+20] Ryan Blair et al. "Kirby-Thompson distance for trisections of knotted surfaces". In: *arXiv preprint arXiv:2002.03991* (2020) (↑ 3, 35).

[CU06] Ildefonso Castro and Francisco Urbano. *Minimal Lagrangian surfaces in $S^2 \times S^2$*. 2006. arXiv: `math/0601637 [math.DG]` (↑ 41).

[Cas+22] Nickolas A Castro et al. "The relative $\mathcal{L}$-invariant of a compact 4-manifold". In: *Pacific Journal of Mathematics* 315.2 (2022), pp. 305–346 (↑ 3, 8, 35).

[DHL19] Bo Dai, Chung-I Ho, and Tian-Jun Li. "Nonorientable Lagrangian surfaces in rational 4-manifolds". In: *Algebraic & Geometric Topology* 19.6 (2019), pp. 2837–2854 (↑ 13).

[GK16] David Gay and Robion Kirby. "Trisecting 4-manifolds". In: *Geometry & Topology* 20.6 (2016), pp. 3097–3132 (↑ 1, 3, 6, 7).

[Giv86] Aleksandr Borisovich Givental. "Lagrangian imbeddings of surfaces and unfolded Whitney umbrella". In: *Functional Analysis and Its Applications* 20.3 (1986), pp. 197–203 (↑ 13).

[GL24] Devashi Gulati and Peter Lambert-Cole. *Moduli Spaces of Lagrangian Surfaces in $\mathbb{CP}^2$ obtained from Triple Grid Diagrams*. 2024. arXiv: 2406.12767 (↑ 2, 14, 44).

[Hem01] John Hempel. "3-manifolds as viewed from the curve complex". In: *Topology. An International Journal of Mathematics* 40.3 (2001), pp. 631–657 (↑ 31).

[IN20] Gabriel Islambouli and Patrick Naylor. "Multisections of 4-manifolds". In: *arXiv preprint arXiv:2010.03057* (2020) (↑ 7, 8, 36).

[Isl+22] Gabriel Islambouli et al. "Toric multisections and curves in rational surfaces". In: *arXiv preprint arXiv:2206.04161* (2022) (↑ 35).

[Joh06] Jesse Johnson. "Heegaard splittings and the pants complex". In: *Algebraic & Geometric Topology* 6.2 (2006), pp. 853–874 (↑ 3).

[KT18] Robion Kirby and Abigail Thompson. "A new invariant of 4-manifolds". In: *Proceedings of the National Academy of Sciences* 115.43 (2018), pp. 10857–10860 (↑ 2).

[Lam21] Peter Lambert-Cole. "An adjunction criterion in almost-complex 4-manifolds". In: 2021 (↑ 4, 42, 47).

[LP72] François Laudenbach and Valentin Poénaru. "A note on 4-dimensional handlebodies". en. In: *Bulletin de la Société Mathématique de France* 100 (1972), pp. 337–344 (↑ 7).

[Mei18] Jeffrey Meier. "Trisections and spun 4-manifolds". In: *Mathematical Research Letters* 25.5 (2018), pp. 1497–1524 (↑ 36).

[MZ17a] Jeffrey Meier and Alexander Zupan. "Bridge trisections of knotted surfaces in S^4". In: *Transactions of the American Mathematical Society* 369.10 (May 2017), pp. 7343–7386 (↑ 2).

[MZ17b] Jeffrey Meier and Alexander Zupan. "Genus-two trisections are standard". In: *Geometry & Topology* 21.3 (2017), pp. 1583–1630 (↑ 36).

[MZ18] Jeffrey Meier and Alexander Zupan. “Bridge trisections of knotted surfaces in 4-manifolds”. In: *Proceedings of the National Academy of Sciences* 115.43 (2018), pp. 10880–10886 (↑ 1, 10).

[Nem09] Stefan Yurievich Nemirovski. “Homology class of a Lagrangian Klein bottle”. In: *Izvestiya: Mathematics* 73.4 (2009), pp. 689–698 (↑ 13).

[Oga21] Masaki Ogawa. “Trisections with Kirby-Thompson length 2”. In: *arXiv preprint arXiv:2112.10033* (2021) (↑ 36).

[She09] Vsevolod V. Shevchishin. “Lagrangian embeddings of the Klein bottle and combinatorial properties of mapping class groups”. In: *Izvestiya: Mathematics* 73.4 (2009), pp. 797–859 (↑ 13).

[Via16] Renato Ferreira de Velloso Vianna. “Infinitely many exotic monotone Lagrangian tori in $\mathbb{CP}^2$”. In: *J. Topol.* 9.2 (2016), pp. 535–551 (↑ 13).

[Zup13] Alexander Zupan. “Bridge and pants complexities of knots”. In: *Journal of the London Mathematical Society* 87.1 (2013), pp. 43–68 (↑ 3, 37).